340
4-16-81
JWR

MASTER

Dr. 2563

DOE/ET/20550-2(Vol.3)

LINE-FOCUS SOLAR CENTRAL POWER SYSTEM—PHASE I

Final Report for September 29, 1978—April 30, 1980, Volume 3: Appendices

By
Arthur J. Slemmons

Dist-270
TIS-23

April 1980

Work Performed Under Contract No. AT03-76ET20550

SRI International
Menlo Park, California

U.S. Department of Energy

Solar Energy

DISTRIBUTION OF THIS DOCUMENT IS UNLIMITED

DISCLAIMER

This report was prepared as an account of work sponsored by an agency of the United States Government. Neither the United States Government nor any agency Thereof, nor any of their employees, makes any warranty, express or implied, or assumes any legal liability or responsibility for the accuracy, completeness, or usefulness of any information, apparatus, product, or process disclosed, or represents that its use would not infringe privately owned rights. Reference herein to any specific commercial product, process, or service by trade name, trademark, manufacturer, or otherwise does not necessarily constitute or imply its endorsement, recommendation, or favoring by the United States Government or any agency thereof. The views and opinions of authors expressed herein do not necessarily state or reflect those of the United States Government or any agency thereof.

DISCLAIMER

Portions of this document may be illegible in electronic image products. Images are produced from the best available original document.

DISCLAIMER

"This book was prepared as an account of work sponsored by an agency of the United States Government. Neither the United States Government nor any agency thereof, nor any of their employees, makes any warranty, express or implied, or assumes any legal liability or responsibility for the accuracy, completeness, or usefulness of any information, apparatus, product, or process disclosed, or represents that its use would not infringe privately owned rights. Reference herein to any specific commercial product, process, or service by trade name, trademark, manufacturer, or otherwise, does not necessarily constitute or imply its endorsement, recommendation, or favoring by the United States Government or any agency thereof. The views and opinions of authors expressed herein do not necessarily state or reflect those of the United States Government or any agency thereof."

This report has been reproduced directly from the best available copy.

Available from the National Technical Information Service, U. S. Department of Commerce, Springfield, Virginia 22161.

Price: Printed Copy A04
Microfiche A01

DOE/ET/20550-2(Vol.3)
Distribution Category UC-62c

LINE-FOCUS SOLAR CENTRAL POWER SYSTEM—PHASE I

Final Report

Volume III: Appendices

April 1980

By: Arthur J. Slemmons, Senior Research Engineer
Engineering Sciences Laboratory

Prepared for:

U.S. Department of Energy
DOE-SAN
333 Broadway
Oakland, California 94612

Attn: Mr. Larry Prince

Contract EY-76-C-03-0115
WO-3-78-482 PA #140

SRI Project 7896

SRI International
333 Ravenswood Avenue
Menlo Park, California 94025

DISTRIBUTION OF THIS DOCUMENT IS UNLIMITED

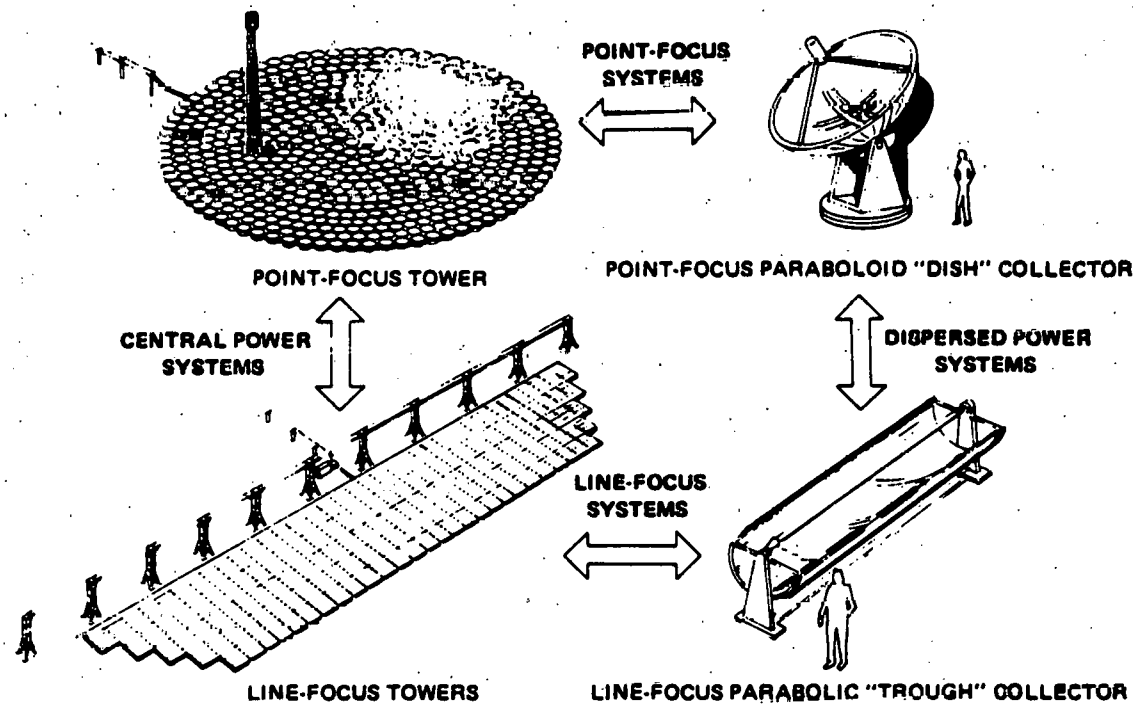

FRONTISPIECE THE FOUR GENERIC TYPES OF SOLAR THERMAL POWER SYSTEMS BEING STUDIED BY THE U.S. DEPARTMENT OF ENERGY

CONTENTS

ILLUSTRATIONS

TABLES

PREFACE

This report is submitted by SRI International to the Department of Energy, under Contract EY-76-C-03-0115, as the final document for the Phase I study of the Line-Focus Central Power System. It contains a summary of the system analysis, parametric analysis, selection and conceptual design of the optimized system, and determination of the commercial market for solar line-focus central power plants.

The report is submitted in three volumes, as follows:

Volume I Executive Overview

Volume II Conceptual Design of the Line-Focus Central Power System

Volume III Appendices

Specific tasks performed by members of the SRI International team were as follows:

- SRI International
  - System analysis
  - System optimization
  - System configuration selection
  - Master control subsystem analysis and selection
  - Receiver subsystem experiments
  - Cost and performance analysis
  - Commercial assessment
- Bechtel National Inc.--Analysis, optimization, selection, and conceptual design of:
  - Heat transport subsystem
  - Energy storage subsystem
  - Electrical power generating subsystem

- Receiver towers
- Heliostat foundations

- Foster Wheeler Development Corporation--Analysis, optimization, selection, and conceptual design of the receiver subsystem
- Acurex/Aerotherm Corporation--Analysis, optimization, selection, and conceptual design of the collector subsystem
- Pacific Gas and Electric Company--Consultant to SRI International

Appendix A

METHODS OF DETERMINATION OF MOLTEN SALT HEAT-TRANSFER COEFFICIENTS AND TUBE-WALL TEMPERATURES

THIS PAGE

WAS INTENTIONALLY

LEFT BLANK

Appendix A

METHODS OF DETERMINATION OF MOLTEN SALT HEAT-TRANSFER COEFFICIENTS AND TUBE-WALL TEMPERATURES

Depending upon the flow regime (laminar, transition or turbulent), one of three equations was used to estimate the molten salt heat transfer coefficient, h_i.

In the laminar flow region (Reynolds numbers less than 2100), the Sieder-Tate equation (eq. A-1) was used (Ref. A-1):

$$h_i = 1.86\ k\ (RePr\ D/L)^{1/3}\ \ (\mu/\mu_\omega)^{0.4}/D \qquad (A-1)$$

The maximum value of h_i allowed in this flow region was calculated as:

$$h_i(max) = (2wC_p)/(\pi DL) \qquad (A-2)$$

If the value of h_i calculated by equation (A-1) exceeds this value, h_i was set equal to $h_i(max)$.

In the transition flow region (Reynolds numbers between 2100 and 10,000) the Hauzen equation (eq. A-2) was used (Ref. A-2):

$$h_i = 0.116\ k(Re^{2/3} - 125)(Pr)^{1/3}(\mu/\mu_\omega)^{0.14}(1 + [D/L]^{2/3})/D \qquad (A-3)$$

In the fully turbulent flow region (Reynolds numbers above 10,000) the Dittus-Boelter equation (eq. A-3) was used (Ref. A-3):

$$h_i = 0.023\ k(Re)^{0.8}(Pr)^{1/3}/D \qquad (A-4)$$

For all three equations, the following definitions apply:

h_i = convective inside heat transfer coefficient, $W/m^2 °C$

Re = Reynolds number = $DV\rho/\mu$, dimensionless

Pr = Prandtl number = $C_p\mu/k$, dimensionless

D = tube inside diameter, m

L = tube length, m

V = flow velocity, m/s

k = molten salt thermal conductivity, W/m°C

ρ = molten salt density, kg/m^3

μ = molten salt viscosity at bulk fluid temperature, kg/ms

μ_ω = molten salt viscosity at tube wall temperature, kg/ms

C_p = molten salt specific heat, Ws/kg°C

Over the region of interest, the temperature difference between the bulk fluid temperature and tube wall temperature is small; therefore, to simplify the calculations, the value of $(\mu/\mu_\omega)^{0.14}$ was taken as equal to 1.0 for all cases.

The appropriate value of the inside heat transfer coefficient, h_i obtained from the above equations was used to determine the inside, outside and average tube wall temperatures. The inside tube wall temperature was determined from the following equation:

$$T_i = T_{out}^* + q/h_i \qquad \text{(A-5)}$$

---

*The molten salt outlet temperature rather than the fluid bulk temperature was used to assure conservative results.

where

T_i = tube inside wall temperature, °C

T_{out} = molten salt outlet temperature, °C

q = heat flux to panel, W/m^2

h_i = convective inside heat transfer coefficient, W/m^2-°C

The temperature drop through the wall was determined by

$$q = k_m \, dT/dx \tag{A-6}$$

which can be rearranged to:

$$dT = q \, dx/k_m \tag{A-7}$$

where

q = heat flux to panel, W/m^2

dx = tube wall thickness, m^2

k_m = mean value of tube metal thermal conductivity, W/m°C

dT = temperature drop through tube wall, °C

T_o = outside wall temperature

The tube metal thermal conductivity was related to temperature by an equation of the form:

$$k = a + bT \tag{A-8}$$

where

k = tube metal thermal conductivity, W/m°C

a,b = constants

T = temperature, °C

The average temperature used to evaluate k_m was taken as the log mean temperature defined by:

$$T_{lm} = (T_o - T_i)/\ln(T_o/T_i) \qquad \text{(A-9)}$$

Using equations (A-7), (A-8), and (A-9), a trial and error procedure was used to calculate the true values of T_o and T_i.

REFERENCES, APPENDIX A

A-1 Sieder, E. N. and Tate, G. E., Ind. Eng. Chem., 28 1429-1436 (1936).

A-2 Hauzen, H., Z Ver. deut Ing. Beiheft Verfahrenstechnik (4) 91-98 (1943).

A-3 Dittus, F. W. and Boelter, L. M. K., Univ. Calif. Pubs. Eng. 2, 443 (1930).

Appendix B

INPUTS FOR STEAEC PROGRAM

THIS PAGE

WAS INTENTIONALLY

LEFT BLANK

Appendix B

INPUTS FOR STEAEC PROGRAM

B.1 TCS--Time Required for a Cold Start

Overnight molten salt is circulated to maintain the receiver at a temperature of 260°C (500°F). At daybreak solar flux is directed onto the receivers until the panel-averaged, full-load temperature of 427°C (800°F) is reached. A cold start is defined as raising the receiver temperature from 260°C (500°F) to 427°C (800°F).

Under these conditions, the energy required to heat the receivers to operating condition is defined as follows:

$$Q(reqd) = \left[(MC_p)_{steel} + (MC_p)_{salt}\right]\Delta t_{cs} \qquad (B\text{-}1)$$

where

$Q(reqd)$ = heat required for a "cold start," MWh

M_{steel} = weight of tubes and fins in receivers, kg

$C_{p\ steel}$ = specific heat of steel, J/kg°C

M_{salt} = weight of salt in tubes in receivers, kg

$C_{p\ salt}$ = specific heat of salt, J/kg°C

Δt_{cs} = cold start temperature change, °C

The following values are substituted into equation (B-1):

Variable	Value
M_{steel}	= 1,013,870 kg (2,235,200 lbm)
$C_{p\ steel}$	= 460.536 J/kg°C (0.11 Btu/lbm°F)
M_{salt}	= 592,755 kg (1,306,800 lbm)
$C_{p\ salt}$	= 1553.26 J/kg°C (0.371 Btu/lbm°F)
Δt	= 167°C (300°F)

The resulting energy is:

$$Q(reqd) = 64.371 \text{ MWh } (219.21 \times 10^6 \text{ Btu})$$

A graph of power to the receivers vs time of day exhibits a slope of 175.5 MW/h (598.76×10^6 Btu/h^2) during the first 1-1/2 hours after sunrise. Thus, the time required for a cold start θ_{cs} is

$$\theta_{cs} = (2Qreqd/slope)^{1/2} = 0.856 \text{ h}$$

B.2 Receiver Cooldown Parameter

An equation similar to equation (B-1) can be written for the receiver heat losses, namely:

$$q(loss) = \left[(MC_p)_{steel} + MC_p)_{salt}\right]\Delta t_{CD}/\Delta\theta_{CD} \qquad (B-2)$$

where

$q(loss)$ = rate of heat loss from receiver, W/s

Δt_{CD} = cooldown temperature drop = $tw_i - t_{amb}$, °C

$\Delta\theta_{CD}$ = cooldown time interval, s

MC_p = as defined for equation (B-1)

tw_i = temperature of receiver inside wall, °C

t_{amb} = ambient outside temperature, °C

The overall heat-transfer losses from the receivers can also be expressed by:

$$q(loss) = U_o A_o \Delta t_{CD}/\Delta\theta_{CD} \qquad (B-3)$$

where

U_o = overall heat-transfer coefficient, $W/m^2°C$

A_o = overall receiver heat-transfer area, m^2

At shutdown, the aperture door is closed, and the overall heat-transfer coefficient, U_o, can be determined from the following equation:

$$U_o = \frac{1}{\frac{r_o \ln(r_o/r_i)}{k_m} + \frac{1}{h_o}} \qquad \text{(B-4)}$$

where

U_o = overall heat-transfer coefficient, $W/m^2°C$

r_i = inside radius of receiver, m

r_o = outside radius of receiver, m

k_m = metal thermal conductivity, $W/m°C$

h_o = outside convection heat-transfer coefficient, $W/m^2°C$

The overall receiver heat-transfer area is as follows:

$$A_o = \underbrace{3/4(2\pi r_o L)}_{\text{Active section}} + \underbrace{1/4(2\pi r_o' L)}_{\text{Aperture cover}} \qquad \text{(B-5)}$$

where

A_o = overall receiver heat-transfer area, m^2

r_i = inside radius of receiver, m

r_o = outside radius of receiver = $r_i + \Delta x$, m

Δx = insulation thickness, m

L = total length of receivers, m

r_o' = aperture cover outside radius = $r_i + \Delta x'$, m

$\Delta x'$ = aperture cover insulation thickness, m

Rearranging and simplifying, equation (B-5) becomes

$$A_o = \pi L(4r_o + 3\Delta x + \Delta x')/2 \qquad \text{(B-5')}$$

The highest heat losses occur when the convective resistance to heat transfer ($1/h_o$) is equal to zero (i.e., when $h_o = \infty$). Substituting this condition into equation (B-2) and simplifying yields:

$$U_o = \frac{k_2}{r_o \ln(r_o/r_i)} \qquad \text{(B-4')}$$

The total heat losses can be related to the cooldown time as follows:

- Initial values of 387°C (728°F) and 27°C (80°F) were selected for tw_o and t_{amb}, respectively.
- A time interval $\Delta\theta_{CD}$ of 300 s was selected.
- The value of q(loss) was obtained from equation (B-3).
- Equation (B-2) was solved for Δt_{CD}.
- A new value of tw_i was obtained by $tw_i' = tw_i - \Delta t_{CD}$.
- The last four steps are repeated until tw_i is less than 260°C (500°F).

XT, a parameter that identifies how far along the cooldown curve the receiver has traveled since shutdown was set, is equal to the losses at any time, divided by the losses at time zero. XT is therefore defined by the following equations:

$$XT(\theta) = q(loss)_\theta / q(loss)_{\theta=0} \qquad \text{(B-6)}$$

$$XT(\theta) = X1\, e^{\alpha_r \theta} \qquad \text{(B-7)}$$

where

α_r = cooldown parameter, h^{-1}

XT values versus time were obtained from equation (B-6) and an exponential curve-fit yielded the following values for X1 and α_r:

$$X1 = 1.00038$$

$$\alpha_r = -0.13655\ h^{-1}$$

Appendix C

DESCRIPTION OF SYSTEM ANALYSIS COMPUTER PROGRAM

THIS PAGE

WAS INTENTIONALLY

LEFT BLANK

Appendix C

DESCRIPTION OF SYSTEM ANALYSIS COMPUTER PROGRAM

The levelized busbar electric cost ($\overline{BBEC}$) for the high-temperature line-focus (HTLF) system is calculated using an SRI computer program, written in ALGOL, resident on the SRI International (SRI) Burroughs 6700. A general flowchart for the program is given in Figure C-1.

The program is initiated with the specifications of the various system parameters. These variables are passed to the optics and receiver analysis subprograms, described later. Table C-1 summarizes these initial specifications.

Once the physical specifications are made, view factors may be calculated. The program then asks for "field multiple," a variable which, for a fixed storage, allows calculation of a system longer than that to meet the nominal 100 MW_e production at 2:00 p.m. winter solstice. In this way, daily capacity factors may be increased for a given storage system, because the system length is multiplied by the field multiple. Any additional energy collected is placed into the ESS for use after direct energy production has terminated.

The computer program calls upon the receiver subprogram at equinox at 2:00 p.m. for the purpose of sizing the system length. The receiver subprogram, in turn, calls upon the optics subprogram to provide the insolation flux through the aperture. An iteration process follows (described in Appendix D), in which the mass flow per unit length of receiver is determined. From the velocity specification, a single value of the losses from free and forced convection is determined for the system length.

The program forms a large iteration loop for three days around the hours of solar production. Starting with sunrise, and ending with

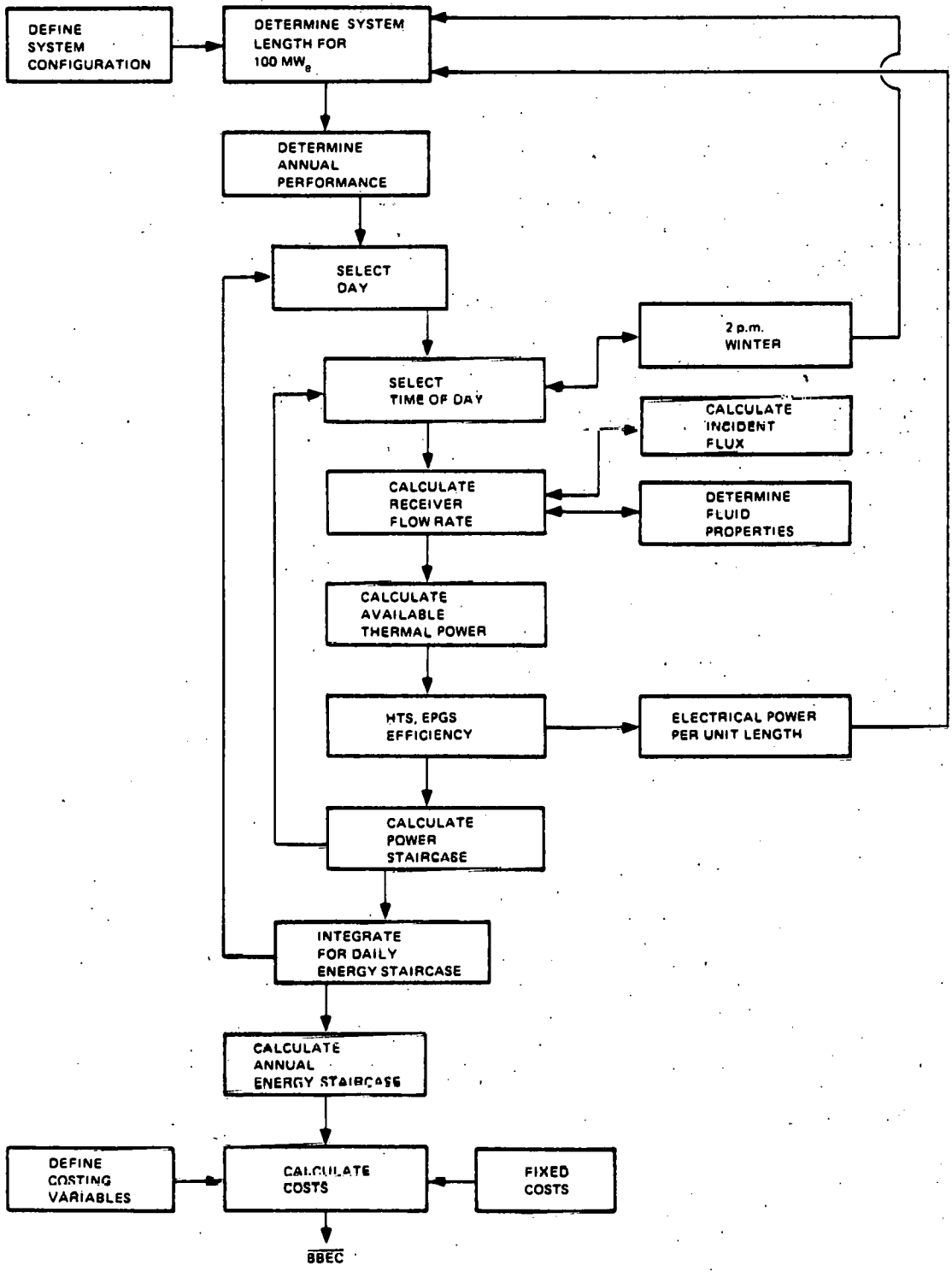

FIGURE C-1 FLOWCHART FOR CALCULATING BUSBAR ENERGY COST ($\overline{BBEC}$)

Table C-1

SYSTEM PARAMETERS

Variable Name	Description	Optics Subprogram	Receiver Subprogram
N	Number of mathematical nodes in receiver	x	x
out	Node for fluid outlet in receiver		x
emissl	Emissivity of reflecting nodes		x
absorpl	Absorptivity of reflective nodes		x
emiss	Emissivity of boiler tubes		x
absorp	Absorptivity of boiler tubes		x
aperture	Aperture width		x
theta	Aperture inclination		x
R	Receiver radius	x	x
pressure	Boiler pressure		x
H_{in}, H_{out}	Inlet and outlet enthalpy		x
tower H	Tower height	x	x
sigmasway	Tower sway	x	x
mirrorw	Mirror width	x	x
nummir	Number of mirror rows	x	x
refl	Mirror reflectivity	x	x
sigma1	Tracking error	x	x
sigma2	Mirror surface error	x	x
velocity	Wind velocity		
focus	Fixed focus or auto focus	x	
season2	Season for fixed focus	x	
time2	Time for fixed focus	x	
allowedstorage	Allowed capacity for ESS	-	-
fieldmultiple	Length multiplier for system size	-	-

sunset, the main program calls the receiver subprogram to provide the mass flow. If for some reason the receiver program solution starts to diverge (at very low flux levels early in the morning) then that data point is skipped, and calculation proceeds to the next hour.

For each hour, the optics subprogram and receiver subprogram provide data arrays that track the power through the system. In particular, a stairstep of the system performance may be created from the following at any hour:

- Power on the mirrors
- Power after cosine loss
- Power after mirror reflection loss
- Power after atmospheric attenuation loss
- Power after heliostat blocking and shading
- Power after receiver shadow loss
- Power after aperture interception loss
- Power after cavity reflection loss
- Power after radiation loss
- Power after convection losses

For each day of calculation, the data from each array is mathematically described by a fourth-order, least-square-fit polynomial. The daily performance is then calculated as a simple arithmetic integration of the polynomials. Figure C-2, parts "a" through "j," shows typical applications of this curve-fitting technique. The values on the right side of the graphs are the fourth-order polynomial coefficients used by the program for integration.

The energy available to the HTS and EPGS is further evaluated as illustrated in Figure C-3. The curve is subdivided into four sections:

- Direct energy, in which the plant is capable of producing 100 $MW_e h$.
- Stored energy, in which energy in excess of that necessary to process 100 $MW_e h$ is sent to the ESS.
- Two portions of optional energy, in which the energy may either be stored, or used in conjunction with energy from the ESS to produce electricity through the EPGS.

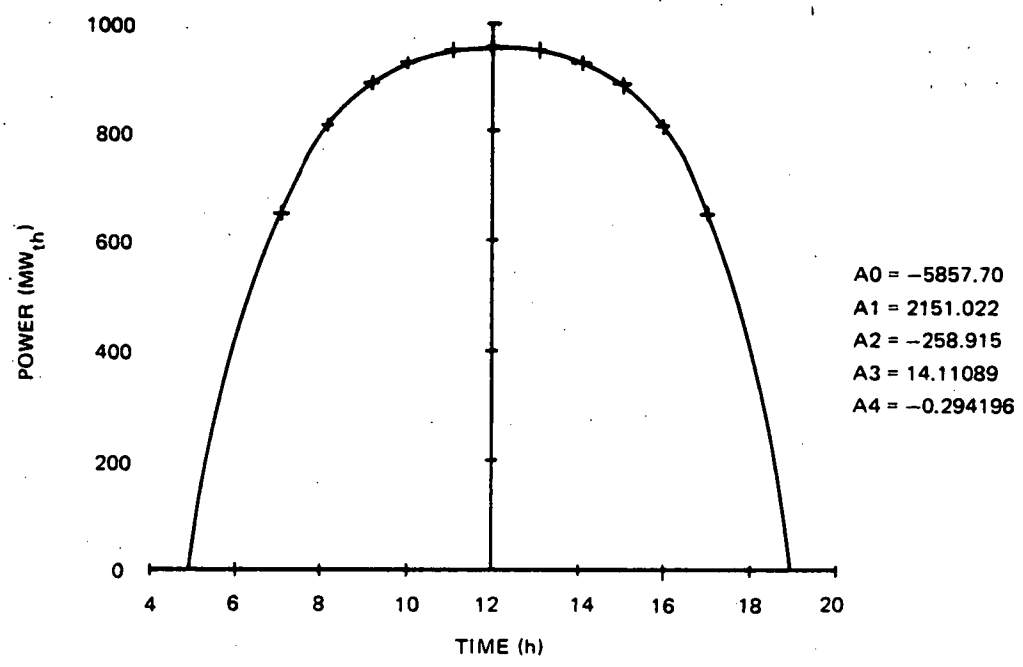

a. POWER ON MIRRORS: SPRING

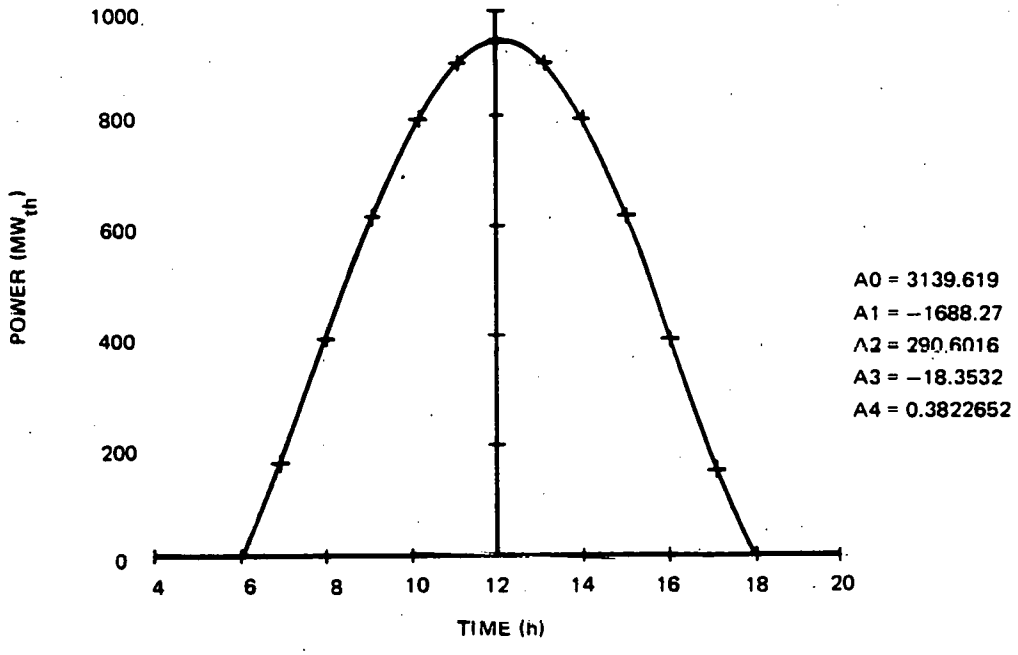

b. POWER AFTER COSINE LOSS: SPRING

FIGURE C-2 DAILY PERFORMANCE CURVES

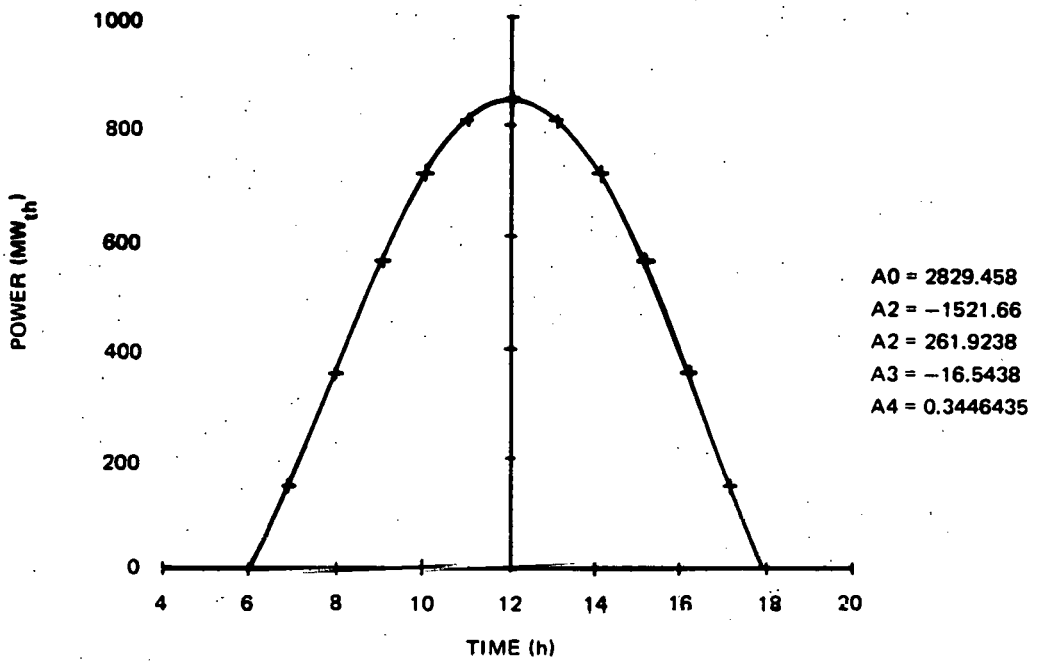

c. POWER AFTER REFLECTION LOSS: SPRING

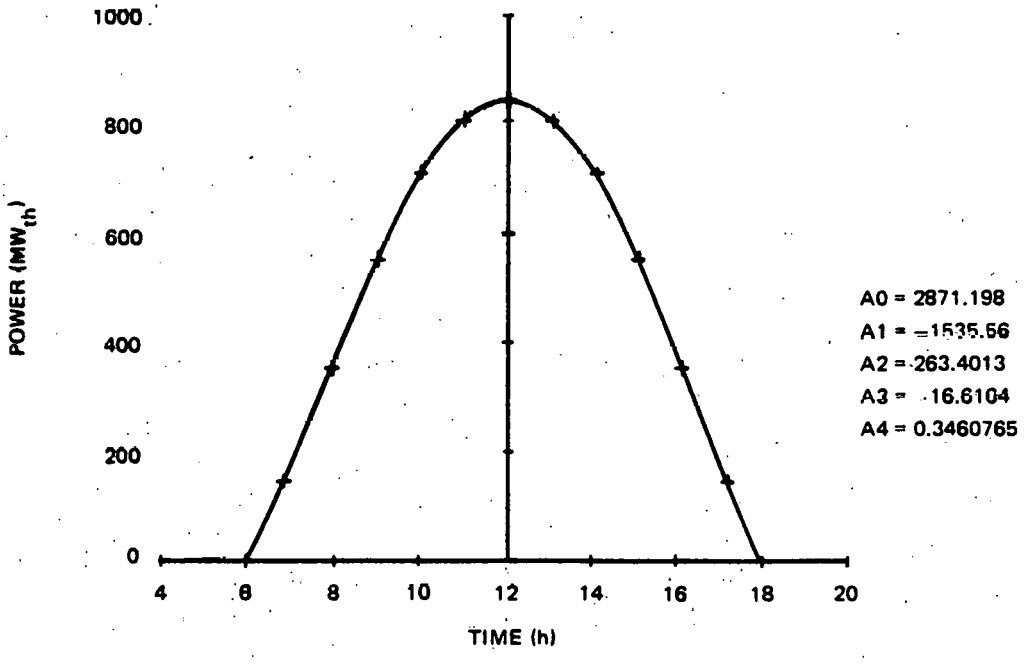

d. POWER AFTER ATTENUATION LOSS: SPRING

FIGURE C-2 (continued)

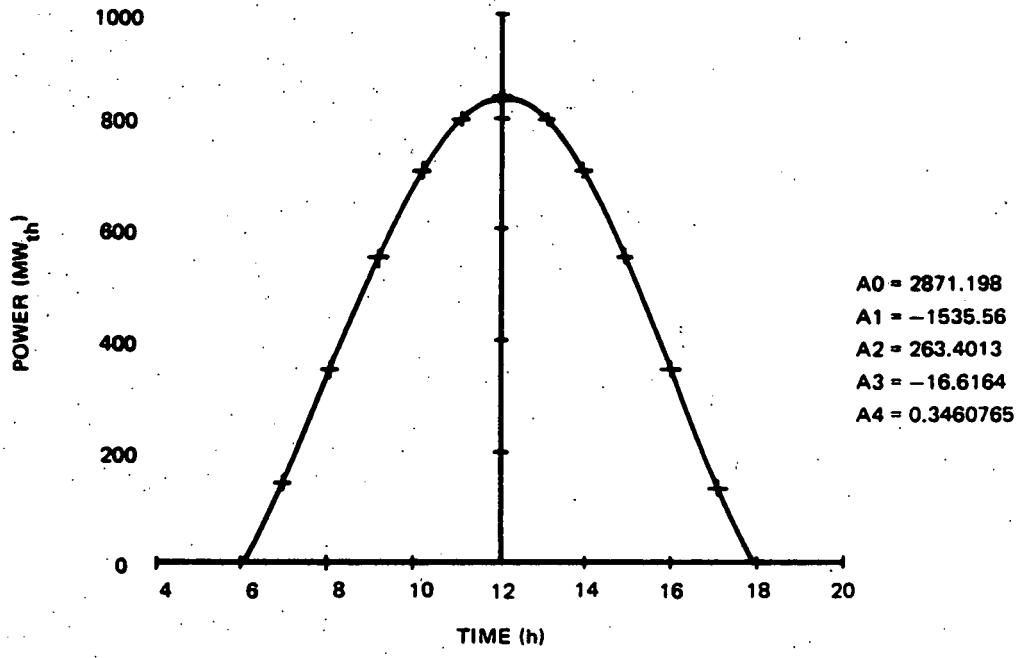

e. POWER AFTER BLOCKING AND SHADING LOSSES: SPRING

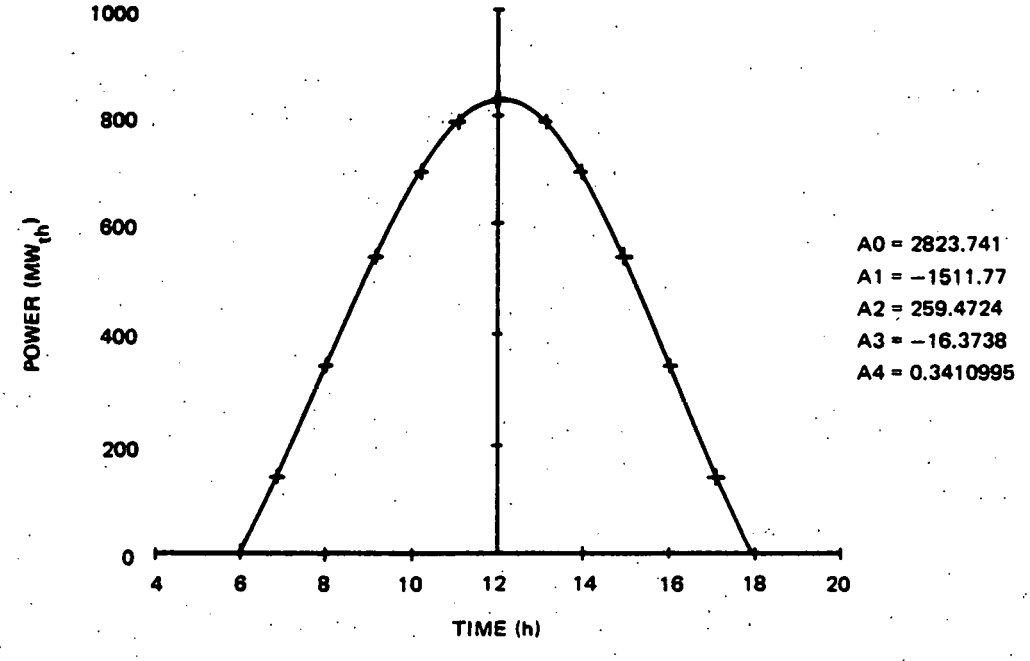

f. POWER AFTER RECEIVER SHADOW LOSS: SPRING

FIGURE C-2 (continued)

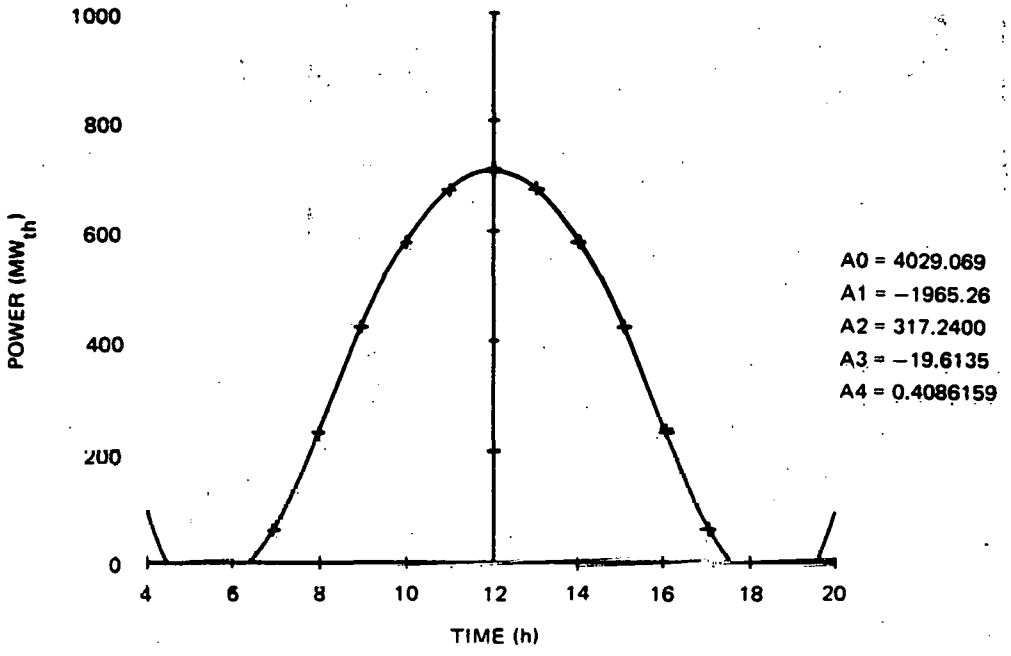

g. POWER AFTER INTERCEPTION LOSS: SPRING

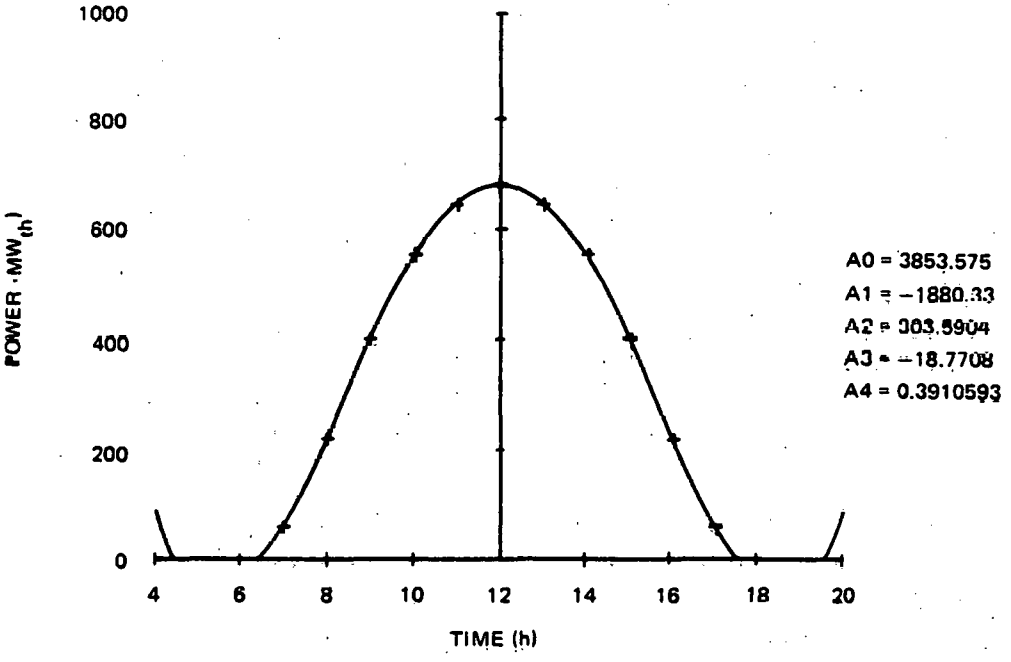

h. POWER AFTER SOLAR REFLECTION LOSSES: SPRING

FIGURE C-2 (continued)

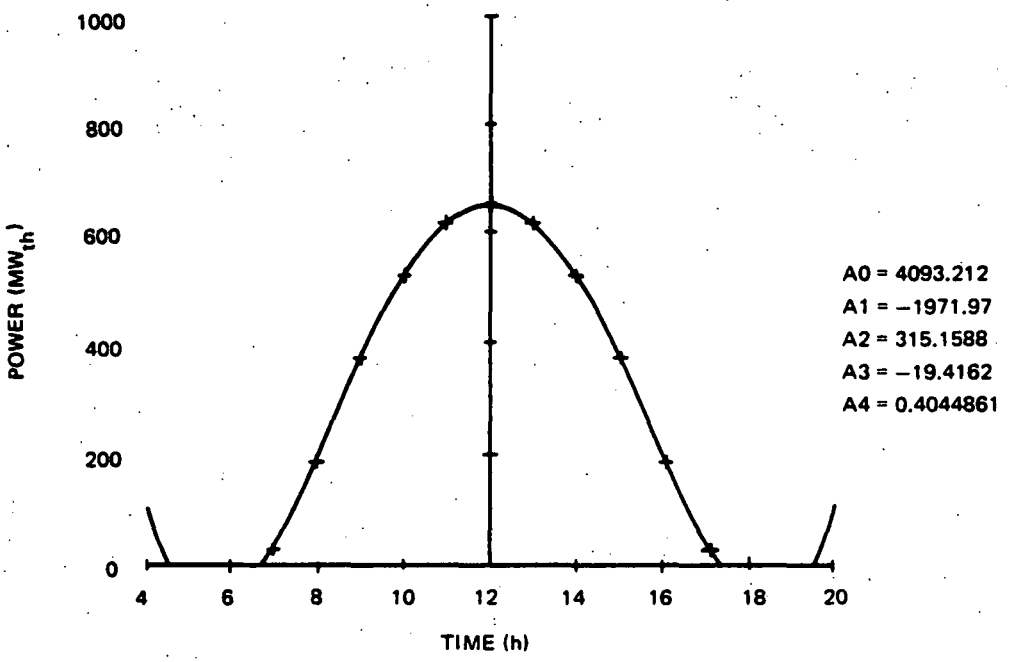

i. POWER AFTER RADIATION LOSSES: SPRING

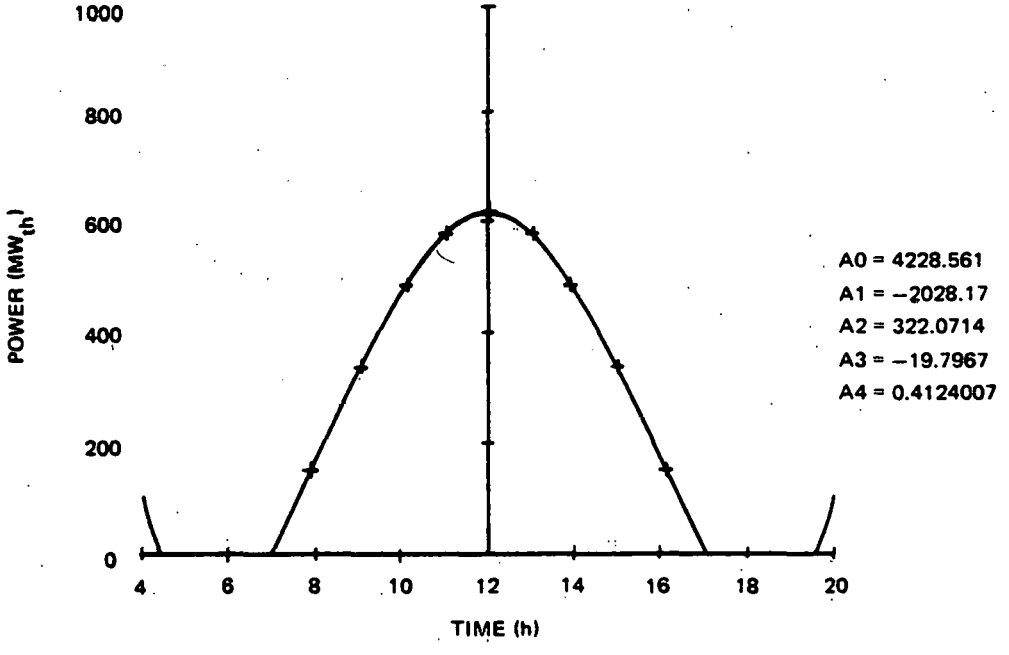

j. POWER AFTER CONVECTION LOSSES: SPRING

FIGURE C-2 (concluded)

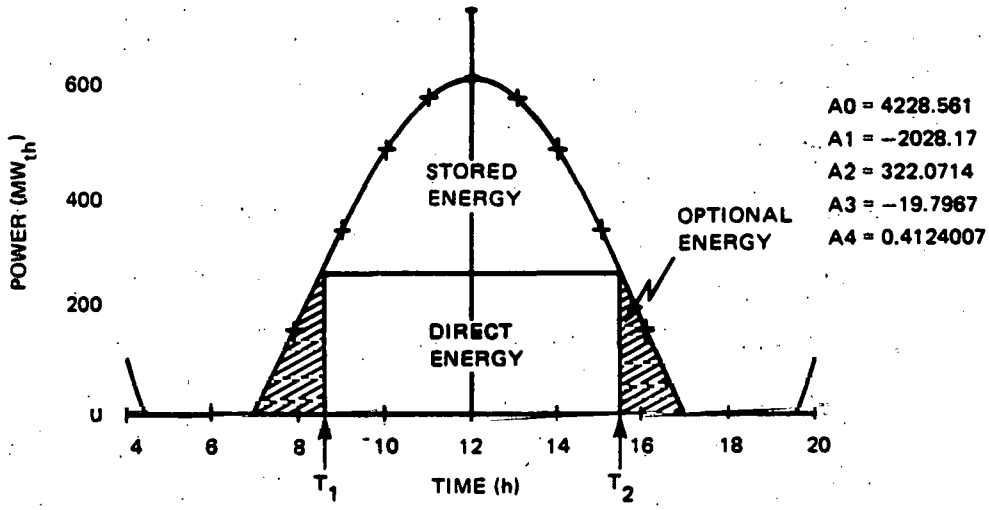

FIGURE C-3 POWER AFTER CONVECTION LOSSES: SPRING

At the completion of power calculations, the main program totals the energies provided by the three days and annualizes the results. The maximum solar multiple from the three days is also reported.

Finally, the main program calls upon the busbar electric costing subprogram. Using the EPRI costing model for present value analysis and cost data and cost parameters, the 30 year levelized busbar electric cost ($\overline{BBEC}$) is calculated. The cost constants in Table C-2 may be readily changed in the program for cost comparison.

The results from each calculation are summarized in a program run typified by Figure C-4.

Table C-2

COST CONSTANTS USED IN CALCULATING BUSBAR ELECTRIC COST

Variable	Default Value
Land cost	\$500/acre
Heliostat cost	\$5.05/ft^2
Receiver cost	\$500/ft
Tower cost	\$132/ft
Structures and improvements	\$39/$kW_e h$
Distributables	\$36/$kW_e h$
BOP	\$38/$kW_e h$
Margin (around site)	400 ft
N rows (field blocks)	16 rows
EPGS width	200 ft
ESS width	100 ft
Turbine pressure	2400 psi

```
SRI INTERNATIONAL   HTLF SOLAR POWER SYSTEM

11:40:39 AM MONDAY, AUGUST 13, 1979

SYSTEM PARAMETERS:

          N=24.0          OUT=14.0        EMISS1=0.7       ABSORP1=0.9
     EMISS=0.06        ABSORP=0.9     APERTURE=4.0        THETA=0.873
          R=3.0     PRESSURE=300.0         HIN=204.0       HOUT=389.0
     TOWERH=60.0       MIRRORW=3.0 MIRRORSP[0]=-5.51311 MIRRORSP[1]=5.358563
MIRRORSP[2]=-.066827 MIRRORSP[3]=.0046657      NUMMIR=24.0        REFL=0.9
     SIGMA1=0.003      SIGMA2=0.0   SIGMASWAY=0.1      VELOCITY=13.4
       FOCUS=0.0     SEASON2=0.0      TIME2=12.0 ALLOWEDSTORAGE=1892.
FIELDMULTIPLE=1.926

TOTAL SYSTEM LENGTH (FT) =     44049.7

WINTER NOON POWER FLOW: (MW)

     MIRRORS            =    923.0
     COSINE LOSS        =    903.9
     REFLECTION         =    813.5
     ATTENUATION        =    805.9
     BLOCKING,SHADING   =    797.8
     RECEIVER SHADOW    =    786.4
     INTERCEPTION       =    736.5
     SOLAR REFLECTION   =    702.5
     RADIATION          =    663.1
     CONVECTION         =    589.6
     ELECTRIC           =    233.7

WINTER PERFORMANCE: (MWHRTH)

     OPTIONAL ENERGY    =     316.5
     DIRECT ENERGY      =    1571.7
     AVAILABLE STORAGE  =    1389.0
     STORED ENERGY      =    1389.0
     CAPACITY FACTOR    =    0.5250

POWER DISTRIBUTION: (MWTH)

     0.0     0.0     0.0     0.0     0.0
     0.0     0.0     0.0    52.0   277.5
   459.6   562.3   589.6   555.4   447.5
   264.0    22.6     0.0     0.0     0.0
```

FIGURE C-4 TYPICAL PROGRAM RUN

```
SRI INTERNATIONAL   HTLF SOLAR POWER SYSTEM


SPRING NOON POWER FLOW: (MW)

     MIRRORS              =     947.4
     COSINE LOSS          =     930.5
     REFLECTION           =     837.4
     ATTENUATION          =     829.7
     BLOCKING,SHADING     =     829.7
     RECEIVER SHADOW      =     818.0
     INTERCEPTION         =     770.5
     SOLAR REFLECTION     =     738.1
     RADIATION            =     694.8
     CONVECTION           =     621.3
     ELECTRIC             =     246.3

SPRING PERFORMANCE: (MWHRTH)

     OPTIONAL ENERGY      =     346.6
     DIRECT ENERGY        =    1741.0
     AVAILABLE STORAGE    =    1655.5
     STORED ENERGY        =    1655.5
     CAPACITY FACTOR      =    0.6023

POWER DISTRIBUTION: (MWTH)

      0.0      0.0      0.0      0.0      0.0
      0.0      0.0    -44.8    132.8    336.1
    491.8    585.1    621.3    589.6    488.7
    336.1    131.4    -49.6      0.0      0.0

SUMMER NOON POWER FLOW: (MW)

     MIRRORS              =     957.0
     COSINE LOSS          =     908.7
     REFLECTION           =     817.9
     ATTENUATION          =     810.3
     BLOCKING,SHADING     =     810.3
     RECEIVER SHADOW      =     798.6
     INTERCEPTION         =     751.5
     SOLAR REFLECTION     =     720.0
     RADIATION            =     677.4
     CONVECTION           =     603.8
     ELECTRIC             =     239.4

SUMMER PERFORMANCE: (MWHRTH)

     OPTIONAL ENERGY      =     433.6
     DIRECT ENERGY        =    1963.1
     AVAILABLE STORAGE    =    1765.0
     STORED ENERGY        =    1765.0
     CAPACITY FACTOR      =    0.6714

POWER DISTRIBUTION: (MWTH)
```

FIGURE C-4 (continued)

```
SRI INTERNATIONAL   HTLF SOLAR POWER SYSTEM

      0.0      0.0      0.0      0.0      0.0
      0.0    -11.1     84.5    236.8    375.4
    497.6    576.5    503.8    579.9    503.8
    383.0    236.8     81.1    -17.9      0.0

ANNUALIZED ENERGY FLOW (MWHR):

     MIRRORS              =   3533599.3
     COSINE LOSS          =   2453529.9
     REFLECTION           =   2208190.8
     ATTENUATION          =   2179764.5
     BLOCKING,SHADING     =   2124963.7
     RECEIVER SHADOW      =   2097477.7
     INTERCEPTION         =   1851621.4
     SOLAR REFLECTION     =   1774045.9
     RADIATION            =   1630585.5
     CONVECTION           =   1326645.1
     ELECTRIC             =    525882.1

EPRI COSTING MODEL:

          LAND=751.78409737        HTSCOST=13529652.6852      STEAMGENCOST=3910630.0
       ESSCOST=11072538.206           EPGSCOST=2.2404E+7          CIT=1620.25379211
            XO=16.202537921                    K=0.08505        CRF=0.093093130112
        FCR=0.15673430087           CIPV=3514.62086855          XPV=785.22079116
            AC=347.44444579

     500.0       5.05      750.0      208.0       39.0
      36.0       38.0      400.0       10.0      200.0
     100.0     2400.0

SUMMARY:

     YEARLY ENERGY (MWHRTH)                  1326645.1
     SOLAR MULTIPLE                            2.463
     YEARLY CAPACITY FACTOR                   0.6003

     BUSS BAR ELECTRIC COST (MILLS/KWHRE)     66.07

EPRI COSTING MODEL:

          LAND=751.78409737        HTSCOST=13529652.6852      STEAMGENCOST=3910630.0
       ESSCOST=11072538.206           EPGSCOST=2.2404E+7          CIT=1481.25038248
            XO=14.8126038248                   K=0.08505        CRF=0.093093130112
        FCR=0.15673430087           CIPV=3213.11925168          XPV=717.8606556
            AC=317.638937287

     500.0       5.05      542.0      132.0       39.0
      36.0       38.0      400.0       10.0      200.0
     100.0     2400.0
```

FIGURE C-4 (continued)

SRI INTERNATIONAL HTLF SOLAR POWER SYSTEM

SUMMARY:

YEARLY ENERGY (MWHRTH)	1326645.1
SOLAR MULTIPLE	2.463
YEARLY CAPACITY FACTOR	0.6003
BUSS BAR ELECTRIC COST (MILLS/KWHRE)	60.40

FIGURE C-4 (concluded)

Appendix D

RECEIVER ANALYSIS PROGRAM

THIS PAGE

WAS INTENTIONALLY

LEFT BLANK

Appendix D

RECEIVER ANALYSIS PROGRAM

This appendix provides a more detailed explanation of the receiver analysis subprogram. As mentioned in the main text, the cavity contains the heat balance of three processes:

- Redistribution of incident solar flux from reflections within the cavity
- Redistribution of long wavelength (infrared) radiation from emission and reflection within the cavity
- Conduction through the tube walls and convection into the working fluid.

The receiver was modeled as a two-dimensional cavity with two circumferential flow paths from each edge of the aperture towards a common exit at the rear of the cavity. The receiver is divided into N equal circumferential segments along the two flow paths.

The first two processes are separated in the following manner: first, the incident solar flux redistribution is calculated; then, this is used as a driving function for the second process. To do so, the net incident solar flux into the j^{th} segment may be expressed as

$$\phi'_j = \varepsilon_{s_j}\phi_j + \varepsilon_s \sum_{i=1}^{N} \left(1 - \varepsilon_{s_j}\right)\phi'_i F_{j-i} \qquad \text{(D-1)}$$

where

ϕ'_j ≡ net incident solar flux falling on node j after redistribution into cavity

ϕ_j ≡ incident solar flux as provided by collector optics subprogram

ε_{s_j} ≡ solar emissivity at j^{th} segment

F_{j-i} ≡ view factor from the j^{th} to the i^{th} segment

The set of equations defined by equation (D-1) may be solved explicity for the ϕ'_j in the following manner:

$$\phi'_j - \varepsilon_{s_j} \sum_{i=1}^{N} \left(1 - \varepsilon_{s_j}\right)\phi'_j F_{j-1} = \varepsilon_{s_j}\phi_j \quad ;$$

expanding:

$$\begin{bmatrix} \phi'_1 \\ \phi'_2 \\ \vdots \\ \phi'_N \end{bmatrix} - \begin{bmatrix} \varepsilon_{s_1}\left[\left(1-\varepsilon_{s_1}\right)\phi'_1 F_{1-1} + \left(1-\varepsilon_{s_2}\right)\phi'_2 F_{1-2} + \cdots + \left(1-\varepsilon_{s_N}\right)\phi'_N F_{1-N}\right] \\ \varepsilon_{s_2}\left[\left(1-\varepsilon_{s_2}\right)\phi'_1 F_{2-1} + \left(1-\varepsilon_{s_2}\right)\phi'_2 F_{2-2} + \cdots + \left(1-\varepsilon_{s_N}\right)\phi'_N F_{2-N}\right] \\ \vdots \\ \varepsilon_{s_N}\left[\left(1-\varepsilon_{s_1}\right)\phi'_1 F_{N-1} + \left(1-\varepsilon_{s_2}\right)\phi'_2 F_{n-2} + \cdots + \left(1-\varepsilon_{s_N}\right)\phi'_N F_{N-N}\right] \end{bmatrix} \equiv \begin{bmatrix} \varepsilon_{s_1}\phi_1 \\ \varepsilon_{s_2}\phi_2 \\ \vdots \\ \varepsilon_{s_N}\phi_N \end{bmatrix}$$

but $F_{i-i} = 0$

$$\therefore \begin{bmatrix} 1 & \varepsilon_{s_1}\left(\varepsilon_{s_2}-1\right)F_{1-2} & \varepsilon_{s_1}\left(\varepsilon_{s_3}-1\right)F_{1-3} & \cdots & \varepsilon_{s_1}\left(\varepsilon_{s_N}-1\right)F_{1-N} \\ \vdots & & & & \\ \varepsilon_{s_N}\left(\varepsilon_{s_1}-1\right)F_{N-1} & \varepsilon_{s_N}\left(\varepsilon_{s_2}-1\right)F_{N-2} & \cdots & & 1 \end{bmatrix} \cdot \begin{bmatrix} \phi'_1 \\ \vdots \\ \phi'_N \end{bmatrix} = \begin{bmatrix} \varepsilon_{s_1}\phi_1 \\ \vdots \\ \varepsilon_{s_N}\phi_N \end{bmatrix}$$

Let the matrix of coefficients $\equiv \mathcal{P}$

and the right-hand side vector $\equiv \phi_s$

then

$$\mathcal{P} \cdot \phi' = \phi_s \qquad \text{(D-2)}$$

and

$$\Phi' = \mathcal{P}^{-1} \cdot \Phi_s \qquad \text{(D-3)}$$

The net incident solar flux may be expressed as the single vector Φ'.

The view factors F_{j-i} are determined using an approximation offered by Hottel* for surfaces which are greatly elongated in one direction, as is the long cylindrical receiver cavity.

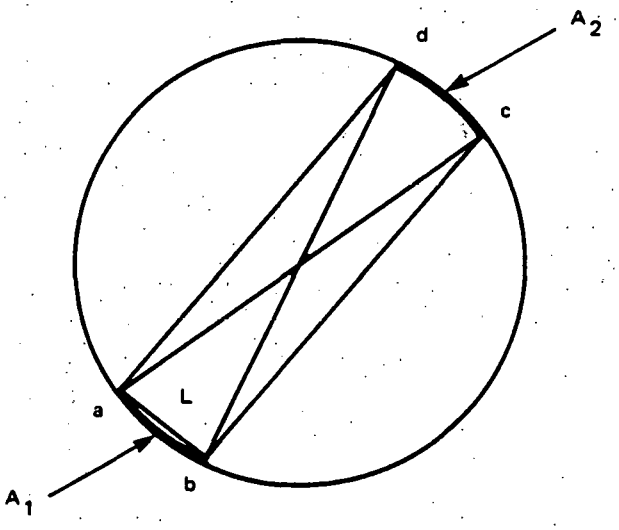

Hottel's method imagines line segments drawn between the endpoints of the two areas A_1 and A_2 for which F_{1-2} is desired. The view factor is then approximated as

*H. C. Hottel, Radiant Heat Transmission, "Heat Transmission," (by W. H. McAdams), 3rd Ed., Ch. 3, McGraw-Hill, Inc., N.Y., 1954.

$$F_{A_1-A_2} = \frac{1}{2L}\left[(\overline{ac} + \overline{bd}) - (\overline{ad} + \overline{bc})\right] \qquad \text{(D-4)}$$

where L is the segment length between area endpoints, and the overbars are the straight-line segments between opposite endpoints.

To make this applicable to the receiver model, the following description is used:

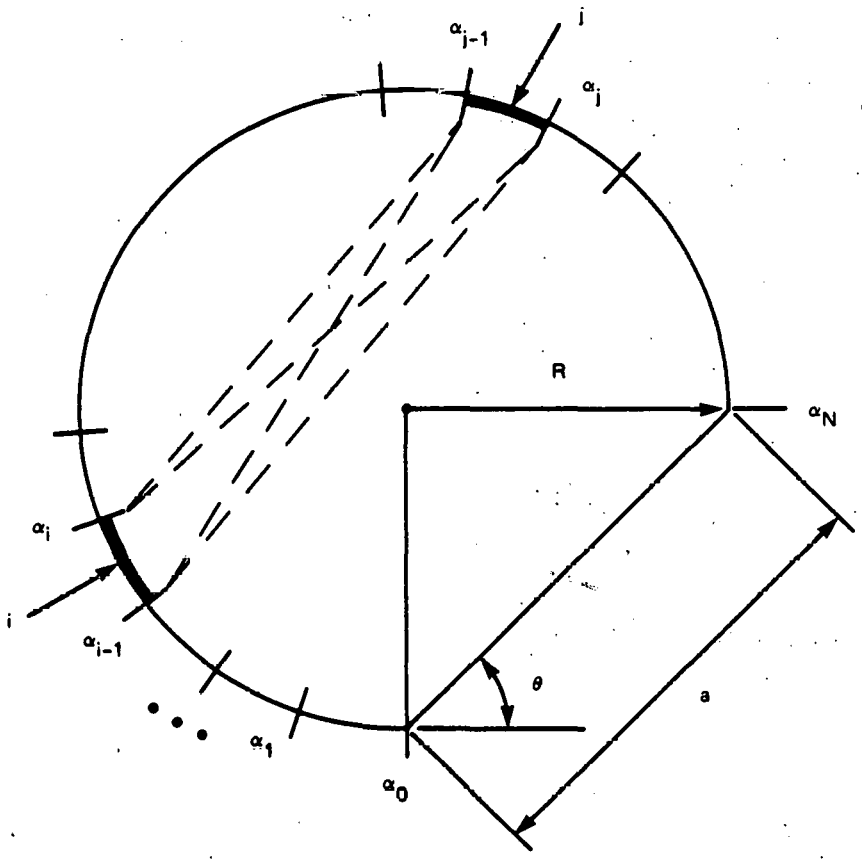

WHERE:
- N = NODES
- a = APERTURE WIDTH
- θ = APERTURE ANGLE
- R = RECEIVER RADIUS

Then the view factor F_{j-i} may be calculated as

$$F_{j-i} = \frac{\sqrt{2}}{2} \frac{1}{2 \sin\left(\frac{\alpha_j - \alpha_{j-1}}{2}\right)} \left\{ \left[1 - \cos\left(\alpha_{i-1} - \alpha_{j-1}\right)\right]^{\frac{1}{2}} + \left[1 - \cos\left(\alpha_i - \alpha_j\right)\right]^{\frac{1}{2}} - \left[1 - \cos\left(\alpha_i - \alpha_{j-1}\right)\right]^{\frac{1}{2}} - \left[1 - \cos\left(\alpha_{i-1} - \alpha_j\right)\right]^{\frac{1}{2}} \right\} \quad \text{(D-5)}$$

The aperture itself is considered a segment as well, and thus may be used mathematically to account for losses through the aperture back into the surroundings.

To address the second process, we employ the following model:

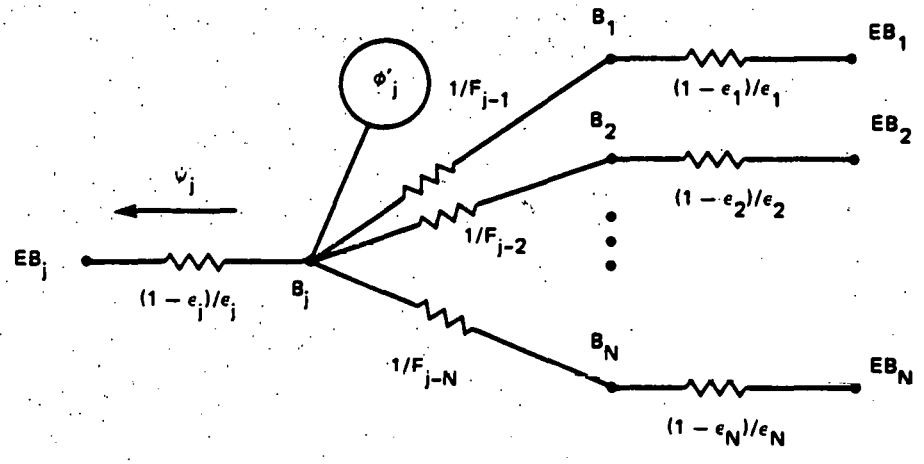

where

B ≡ radiosity

EB ≡ emissive power of a black body (σT^4)

ε ≡ emissivity

Note that the net incident solar flux is modeled as a "current source" to the j^{th} segmental node.

The flux of radiant energy leaving a surface is the sum of the emitted radiation plus the reflected radiation:

$$B_j = \varepsilon_j \sigma T_j^4 + 1 - \varepsilon_j \sum_{i=1}^{N} B_i F_{j-i} \qquad \text{(D-6)}$$

Remember that we have removed the high energy solar flux term.

The net energy upon the surface is the difference between the radiosity and the irradiation (the total radiation incident upon the surface per unit time per unit area).

$$\psi_j = \sum_{i=1}^{N} B_i F_{j-i} + \phi'_j - B_j \qquad \text{(D-7)}$$

substituting equation (D-6) into equation (D-7)

$$\psi_j = \varepsilon_j \sum_{i=1}^{N} B_i F_{j-i} + \phi'_j - \varepsilon_j \sigma T_j^4 \qquad \text{(D-8)}$$

To express the radiosities as a function of temperature, rearrange equation (D-6):

$$B_j - (1 - \varepsilon_j) \sum_{i=1}^{N} B_i F_{j-i} = \varepsilon_j \sigma T_j^4 \quad ;$$

Expanding:

$$\begin{bmatrix} B_1 \\ B_2 \\ \vdots \\ B_N \end{bmatrix} - \begin{bmatrix} (1-\varepsilon_1)\left[B_1F_{1-1} + B_2F_{1-2} + \cdots + B_NF_{1-N}\right] \\ (1-\varepsilon_2)\left[B_1F_{2-1} + B_2F_{2-2} + \cdots + B_NF_{2-N}\right] \\ \vdots \\ (1-\varepsilon_N)\left[B_NF_{N-1} + B_2F_{N-2} + \cdots + B_NF_{N-N}\right] \end{bmatrix} = \begin{bmatrix} \varepsilon_1\sigma T_1^4 \\ \varepsilon_2\sigma T_2^4 \\ \vdots \\ \varepsilon_N\sigma T_N^4 \end{bmatrix}$$

but $F_{i-i} = 0$

Therefore,

$$\begin{bmatrix} 1 & (\varepsilon_1-1)F_{1-2} & (\varepsilon_1-1)F_{1-3} & \cdots & (\varepsilon_1-1)F_{1-N} \\ (\varepsilon_2-1)F_{2-1} & 1 & (\varepsilon_2-1)F_{2-3} & \cdots & (\varepsilon_2-1)F_{2-N} \\ \vdots & & & & \\ (\varepsilon_N-1)F_{N-1} & (\varepsilon_N-1)F_{N-2} & \cdots & & 1 \end{bmatrix} \cdot \begin{bmatrix} B_1 \\ B_2 \\ \vdots \\ B_N \end{bmatrix} = \begin{bmatrix} \varepsilon_1\sigma T_1^4 \\ \varepsilon_2\sigma T_2^4 \\ \vdots \\ \varepsilon_N\sigma T_N^4 \end{bmatrix}$$

Let coefficient matrix $\equiv \mathcal{A}$

right-hand side vector $\equiv \mathcal{B}$

then $\mathcal{A} \cdot \beta = \mathcal{B}$

and $\beta = \mathcal{A}^{-1} \cdot \mathcal{B}$ (D-9)

Thus, given the temperature distribution, equation (D-9) allows calculation of the radiosity vector β. This knowledge allows calculation of the net flux vector using equation (D-8).

The mathematical model of the receiver assumes that the salt flows in circumferential paths from the two edges of the aperture to a common exit at the back of the receiver:

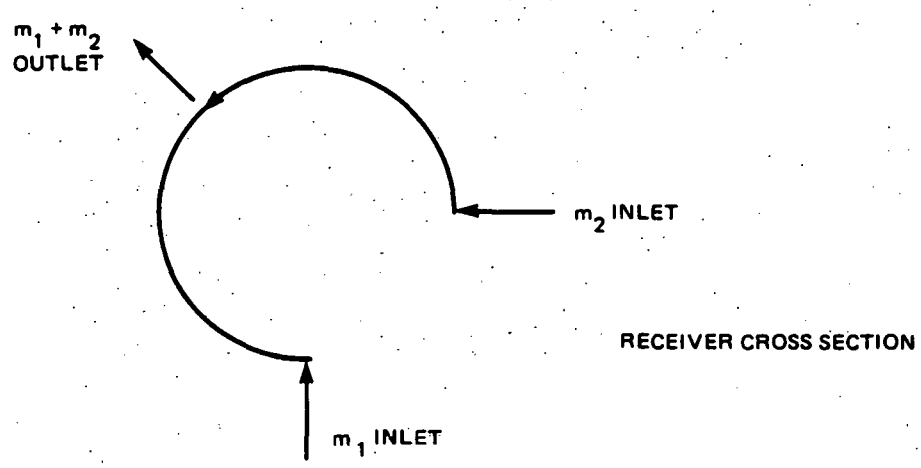

Equation (D-8) provides us the complex relationship between the temperature and the net flux within the cavity. We will use this and the boundary conditions of salt temperature and pressure at the inlet and outlet of the receiver to calculate the solution.

First, we assume for a first approximation that the net flux vector ψ is equal to ϕ', the net incident solar flux. The two flow rates are calculated from the relationships

$$\dot{m}_1 = \frac{1}{\Delta H} \int_{s_1} \psi(s)ds \quad ; \quad \dot{m}_2 = \frac{1}{\Delta H} \int_{s_2} \psi(s)ds \qquad \text{(D-10)}$$

where

s_1 = flow path 1

s_2 = flow path 2

ΔH = enthalpy difference from inlet to outlet

m = mass flow

The enthalpy distribution along the flow path is calculated as

$$H_j = H_{j-1} + \frac{\psi_j s_j}{\dot{m}} \qquad \text{(D-11)}$$

where

H_j = enthalpy at node j

s_j = segment length at node j

An average bulk fluid temperature for each node is determined by the thermodynamic properties of pressure and enthalpy.

$$T_{f_j} = \mathfrak{F}\left(P_{f_j}, \frac{H_j + H_{j-1}}{2}\right) \qquad \text{(D-12)}$$

where

T_{f_j} = bulk fluid temperature at node j

P_{f_j} = pressure at node j

The inside wall temperature follows from the heat transfer relationship:

$$\psi_j = h_f\left(T_{\omega_j} - T_{f_j}\right) \qquad \text{(D-13)}$$

where

h_f = fluid heat transfer coefficient

T_{ω_j} = inside wall temperature

The outside wall temperature follows from the heat conductivity relationship:

$$\psi_j = \left(\frac{k_w}{t}\right)\left(T_{w_j} - T_{\omega_j}\right) \qquad \text{(D-14)}$$

where

k_w = conductivity of boiler pipe

t = thickness of tube wall

T_{w_j} = outside wall temperature

Returning to equations (D-8) and (D-9), the net flux distribution is calculated from the updated temperature vector T_w. An iteration loop consisting of equations (D-10) through (D-14) and (D-8) and (D-9) follows until the net flux vector ψ converges within an established criteria.

To further complicate the process, the final receiver design prescribes the flow inlet for the bottom flow path at node 6 because nodes 1 through 5 provide no appreciable influx of energy. The behavior of this design is analyzed in the following paragraphs.

Nodes 1 through 5 are considered total reflecting and reradiating; i.e., there is no path for energy transmission nor for energy storage. The temperature of the segment rises to the value that balances the incoming flux from reflections within the cavity with the efflux from radiation to other nodes within the cavity.

Because there is no flux transmission into a working fluid for these nodes, equation (D-8), which still describes the radiation behavior at that node, takes a much simpler form:

$$\psi_j = 0 = \varepsilon_j \sum_{i=1}^{N} B_i F_{j-i} + \phi'_j - \varepsilon_j \sigma T_j^4 \qquad \text{(D-8')}$$

Thus, the temperature which balances the incoming and outgoing fluxes becomes:

$$\varepsilon_j \sigma T_j^4 = \phi'_j + \varepsilon_j \sum_{i=1}^{N} B_i F_{j-i} \qquad \text{(D-15)}$$

This modification is incorporated into the iterative process for solution of the receiver performance. After a temperature profile has been calculated from equation (D-14) for those nodal segments in the salt flow path, the radiosities are calculated as prescribed by equation (D-9). The temperatures for nodes 1 through 5 are adjusted per equation (D-15) so that when the net heat fluxes are evaluated (eq. D-8), there is no net flux into nodes 1 through 5, and the energy has been "redistributed" into the other nodes, as the mathematical model would predict.

As before, the iteration process continues until the ψ vector converges within an established criterion.

Figure D-1 is a typical summary of the solution of a receiver subprogram calculation. The performance at 2:00 p.m. winter solstice is determined for the initial specifications listed at the top of the page. The receiver, partitioned into 24 segmental nodes, the first five of which were reflecting only, had salt entering at nodes 6 and 24 and flowing circumferentially towards node 14. Node 25 described the losses through the aperture. The columns "Phi" and "Phim" summarize the incident solar flux and the redistributed solar flux, respectively. TF summarizes the bulk fluid temperature at each node, TWR indicates the outside wall temperature, and PSI yields the net flux into the salt at each node. The mass flow rates for each flow path (in lbm/hr/ receiver foot) are indicated at the bottom of the page.

Figures D-2 through D-4 show the flux absorbed by the receiver for the various seasons. Figures D-5 through D-7 show the thermal power delivered for the various seasons.

RECEIVER DESIGN:		COLLECTOR DESIGN:		INITIAL CONDITIONS:	
APERTURE =	4	MIRROR WIDTH =	3	PRESSURE =	300
THETA =	0.873	# OF MIRRORS =	24	TAMBIENT =	50
RADIUS =	3			H INLET =	204
HEIGHT =	60	SEASON = WINTER		H OUTLET =	389

NODE	E	ES	PHI	PHIM	TF	TWR	PSI
1	0.7	0.9	0	290.301	0	386.57	0
2	0.7	0.9	0	280.659	0	380.99	0
3	0.7	0.9	0	268.440	0	373.70	0
4	0.7	0.9	0	253.757	0	364.62	0
5	0.7	0.9	0	236.743	0	353.67	0
6	0.06	0.9	332.458	516.767	553.26	554.63	431.398
7	0.06	0.9	1246.06	1318.09	566.27	570.18	1224.78
8	0.06	0.9	2420.48	2353.37	593.53	600.69	2244.66
9	0.06	0.9	3764.57	3541.73	637.94	648.81	3406.75
10	0.06	0.9	5177.02	4793.87	700.98	715.70	4616.34
11	0.06	0.9	6601.15	6058.32	782.95	801.49	5816.66
12	0.06	0.9	7857.80	7178.96	882.35	904.15	6838.94
13	0.06	0.9	8371.88	7632.76	992.29	1015.1	7163.50
14	0.06	0.9	7844.74	7157.38	1001.4	1022.7	6677.86
15	0.06	0.9	7101.99	6493.49	911.11	930.64	6126.51
16	0.06	0.9	6116.05	5615.59	830.22	847.23	5333.26
17	0.06	0.9	5257.83	4856.62	759.82	774.61	4636.19
18	0.06	0.9	4730.90	4398.87	697.24	710.72	4224.93
19	0.06	0.9	3664.29	3458.17	643.95	654.54	3319.39
20	0.06	0.9	2446.89	2383.79	604.48	611.72	2268.27
21	0.06	0.9	1417.62	1477.85	578.71	583.11	1377.77
22	0.06	0.9	681.838	835.965	563.70	566.08	744.608
23	0.06	0.9	250.821	466.883	555.74	556.95	380.555
24	0.06	0.9	55.2994	307.736	551.45	552.17	224.543
25	1.00	1.00	0	0	0	50	377.422

TIME OF DAY : 14

TOTAL INCIDENT ENERGY =	45350.87
SOLAR REFLECTION LOSSES =	1906.193
RERADIATION LOSSES =	1509.688
RECEIVER EFFICIENCY =	.8900608

```
**********************
*                    *
* M1DOT =103.32401   *
* M2DOT =115.01655   *
* MDOT  =218.34056   *
*                    *
**********************
```

FIGURE D-1 TYPICAL SUMMARY FROM RECEIVER SUBPROGRAM CALCULATION

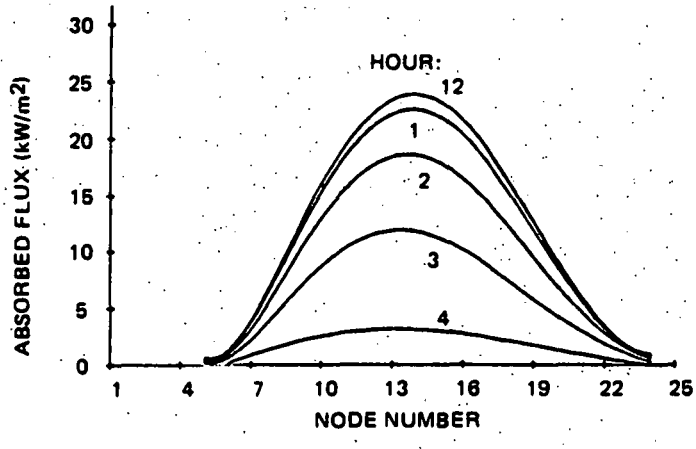

FIGURE D-2 RECEIVER FLUX MAP: WINTER

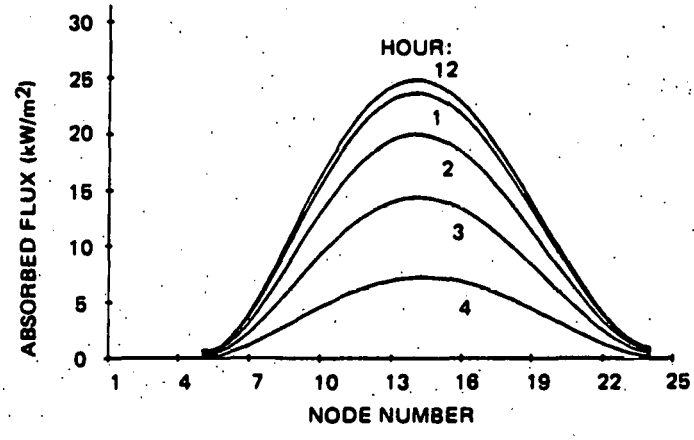

FIGURE D-3 RECEIVER FLUX MAP: SPRING

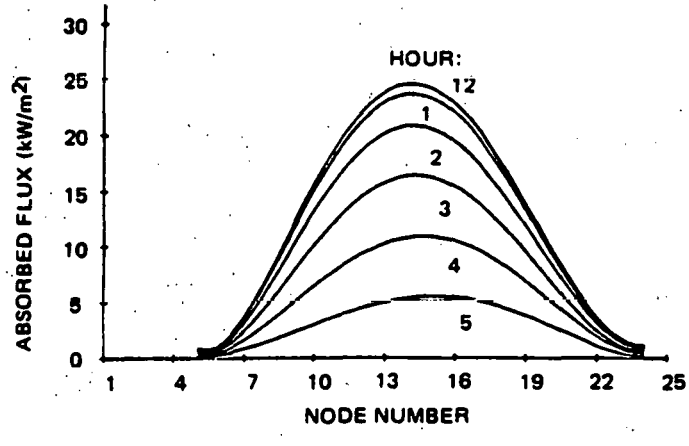

FIGURE D-4 RECEIVER FLUX MAP: SUMMER

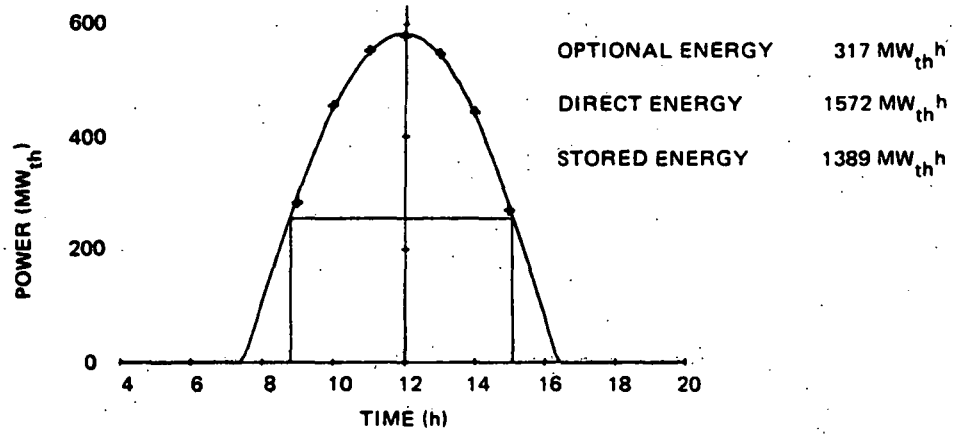

FIGURE D-5 DAILY PERFORMANCE OF RECEIVER: WINTER

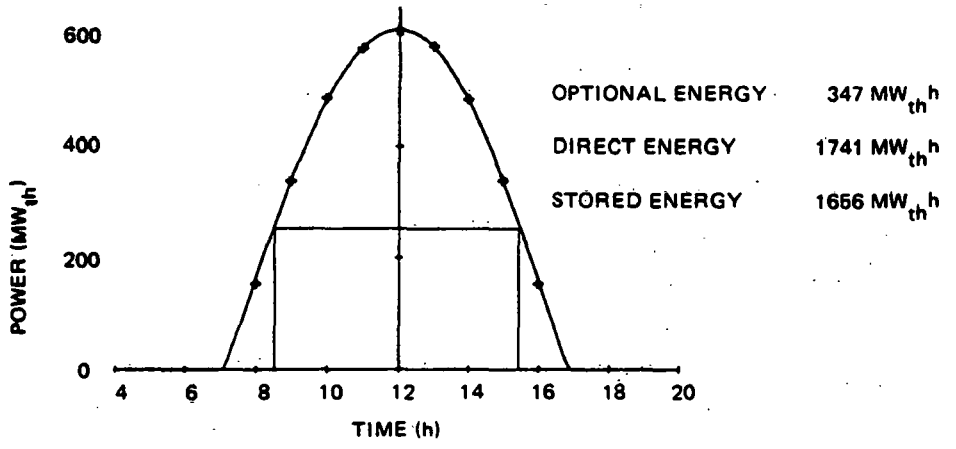

FIGURE D-6 DAILY PERFORMANCE OF RECEIVER: SPRING

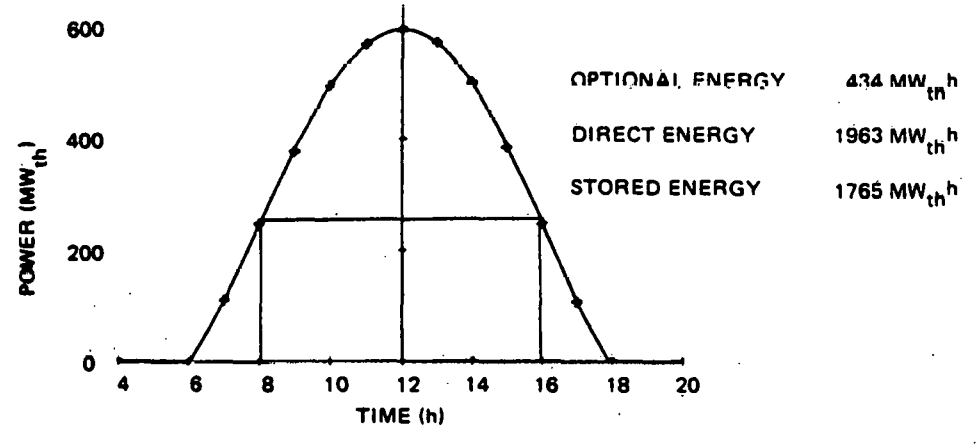

FIGURE D-7 DAILY PERFORMANCE OF RECEIVER: SUMMER

Appendix E

HELIOSTAT PRODUCTION PLAN AND DESIGN METHODOLOGY

THIS PAGE

WAS INTENTIONALLY

LEFT BLANK

Appendix E

HELIOSTAT PRODUCTION PLAN AND DESIGN METHODOLOGY

E.1 Summary

E.1.1 Reflective Panel Production Plan

The costing methodology and detailed planning used to generate cost estimates for labor, bulk materials, indirect charges and tooling are contained in Acurex Final Report No. 79-340, "Low Cost Point-Focus Solar Concentrator, Phase I Final Report."

E.1.2 Drive Subassembly Plan

The general approach for the drive subassembly plan can be shown as follows:

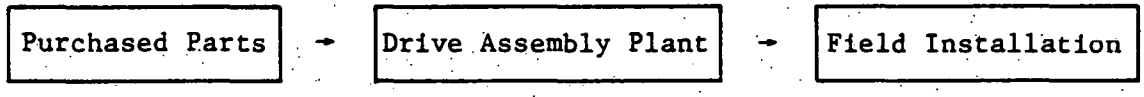

The production cost summary, based on a drive subassembly including module support bearing for a four-module heliostat (1600 ft^2), is shown in Table E-1.

E.1.3 GRC Production Plan

The general approach for the GRC production plan can be shown as follows:

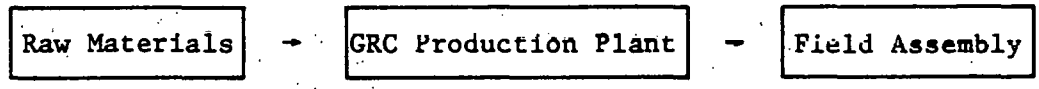

The plant direct-labor requirements are shown in Table E-2.

Direct material requirements are listed in Table E-3.

Table E-1

PRODUCTION COST SUMMARY

Component	Weight/Qty (lb) (ea)	Unit Cost	Cost ($) Labor	Material	Equip.	Indirects	Total Cost ($)
Ballscrew	100/1	$255.00		255		8	263
Motor	45/1	381.00		313		12	393
R-C network	2/1	34.00		34		1	35
Ballscrew anchor	3/1	1.00/lb		3			3
Input crank	79/1	0.60/lb	2	38	3	4	47
Link	3/1	0.60/lb		2		1	3
Output crank	29/1	0.60/lb	1	14	1	1	17
Mount	100/1	0.60/lb	3	48	3	6	60
Caisson cap	10/1	0.60/lb	1	4		1	6
Pivot bolts	2/4	0.50/ea		2			2
Mounting bolts	1/8	0.12/ea		1			1
Incremental encoder	2/1	53.00/ea		53		2	55
Pivots, bearings	20/5	23.40/ea		114		3	117
Assembly of drive	2.2 h	6.00/h	13			33	46
			$20	949	7	72	1048

$$\text{Drive cost} = \frac{\$1048}{1600\ \text{ft}^2} = \$0.65/\text{ft}^2$$

Table E-2

DIRECT-LABOR REQUIREMENTS FOR GRC PRODUCTION PLAN

Station	Stations	Men	Manhours/Module
Incoming material	3	12	1.0
Bulk material mixing	1	4	0.33
Gunnite	2	6	0.50
Press/mold	2	6	0.50
Dewater	2	6	0.50
Steam cure	1	6	0.50
Demold/deflash	1	4	0.33
Assembly fixture	2	6	0.50
Packaging	1	4	0.34
	15	54	4.50

Assumptions: Manufacturing labor rate $4/h ($1979)

2 shifts/day, 250 days/yr

Personal fatigue and delay factor = 0.88

Plant capacity factor = 0.88

Scrap factor = 2%

Overall plant output is 43,200 tubes/yr (17.3 million ft^2/yr)

Manufacturing labor cost: (4.5 h/tube) ($4/h)/400 ft^2 = $0.05 ft^2

Table E-3

DIRECT MATERIAL REQUIREMENTS FOR GRC PRODUCTION PLAN

Component	Qty/Module (lb)	Unit Cost (per lb)	Total Cost/ Module
GRC (cement, water, sand, glass fiber)	3100	$90/$yd^3$ = $0.03	$ 93.00
Tension rods, 3/8 in dia., 3 ea	45	$0.30	13.50
Spider hubs C610.5	158	$0.30	47.40
			$153.90

Equipment and tooling requirements are listed in Table E-4.

Table E-4

EQUIPMENT AND TOOLING REQUIREMENTS FOR GRC PRODUCTION PLAN

Station	Tooling/Equipment	Tools/ Equipment	Unit Cost ($M)	Total Cost ($M)
Incoming bulk material	Material handling/ mixing equipment	3	0.67	2
Gunnite molds	Gunnite fixture	2	1	2
Press molds	Presses, platens	2	3	6
Dewater	Vacuum equipment	2	0.25	0.5
Steam cure	Steam chamber	1	2	2
Demold/deflash	Crane, support fixture	1	1	1
Tube assembly	Assembly fixture	2	0.25	0.5
Packaging	Package fixtures, conveyor	1	1	1
		14		15

Assumptions: 10-yr equipment life

8% cost of capital CRF = 0.149

$$\text{Tooling and equipment cost} = \frac{(0.149)(\$15M)}{43{,}200 \text{ tubes/yr}} = \$52/\text{tube}$$

$\$0.13/ft^2$

Indirect requirements are based on Acurex point-focus heliostat (100,000 heliostats per year production rate). Overhead rate is 147% of direct manufacturing labor. Rate includes:

- Variable indirect labor
  - Supervision
  - Engineering
  - QA
  - Traffic
  - Maintenance

- Nonvariable indirect labor
  - Management
  - Accounting
  - Purchasing
  - Personnel
  - Shipping/receiving
- Fringes
- Facilities
- Process energy
- Indirect materials, consumables

E.1.4 Field Assembly Plan

Field installation is performed by standard crews of six men, one crane operator (split between three crews), four millwrights (an electrician is substituted for wiring connection) and one foreman. Table E-5 summarizes the labor, material and equipment requirements.

E.2 Heliostat Reflective Panel Sizing

The heliostat reflective panel is a 10 ft by 10 ft SMC/flexglass panel with isogrid backing. The panel is line supported at minimum deflection points (one-quarter span locations). The analysis is based on "Isogrid Design Handbook," McDonnell Douglas Astronautics Company, February 1973.

Grid Dimensions:

a = 6.00 in
h = 5.197 in
b = 0.116 (avg) in
d = 2.17 in
t = 0.10 in

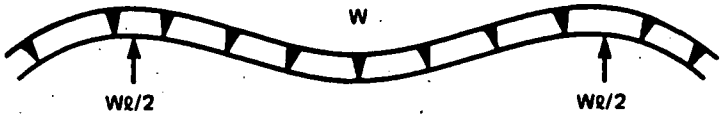

Table E-5

SUMMARY OF REQUIREMENTS FOR FIELD ASSEMBLY PLAN

Operation	Fixed Time Required (h)	Labor Hours	Cost $			
			Labor	Material	Equipment	Indirect
Offload	0.5	3	30			27
Attach pivot bearing	0.5	3	30	25		27
Mount drive unit	1	4	40	5		34
Rig, attach torque tube	2	15	150		24	129
Rig, attach panel	2	15	150	10	40	129
Align panels	1	5	50			43
Electrical connections	0.5	1	10	5		9
Completion tests	0.5	2	20	3		18
			480	48	64	416

$$\text{Installation cost} = \frac{\$1008}{1600\ \text{ft}^2} = \$0.63/\text{ft}^2$$

Loading:

$w = W_{wt} + W_{wind}$

$= (0.67 lb/in^3)$ $t(1 + 3\alpha)$ $+ 0.0033$ lb/in

$= 0.016 + 0.0033$

$= 0.0177$ lb/in^2 =

2.84 lb/ft^2

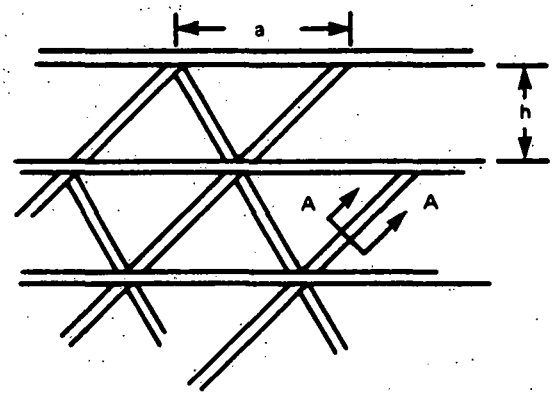

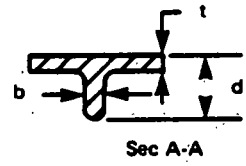

$$\alpha = \frac{bd}{th} = \frac{(0.116)2.17}{(0.10)5.196} = 0.484$$

$$\delta = \frac{d}{t} = \frac{2.17}{0.17} = 21.7$$

$$\beta = \left[3\alpha(1 + \delta)^2 + (1 + \alpha)\ (1 + \alpha\delta^2)\right]^{1/2} = 32.93$$

$$E^* = \frac{(1 + 0.484)^2}{32.98} E = 0.0668E = 86,800 \text{ lb/in}^2$$

$$t^* = \left(\frac{\beta}{1 + \alpha}\right) t = 2.222$$

$$D = \frac{E^* t^{*3}}{12(1 - n^2)} = 84,686$$

Panel Deflection:

$$\Theta_{max} = \frac{w\ell^3}{648\ D} = \frac{(0.0197)(120)^3}{648(84,686)} = 0.6 \text{ mr}$$

E.3 Heliostat GRC Tube Sizing

Tube sizing starts with an equilteral triangular shape which is then reduced in altitude to the minimum required strength and/or stiffness, using altitude/base ratios of 1, 2/3, 1/2 and 1/3. The loads are summarized in Table E-6.

Table E-6

LOAD SUMMARY FOR HELIOSTAT GRC TUBE SIZING

Wind Speed (mph)	Lateral Load (lb/in)	Torque (in-lb)
10	0.3	227
39	4.7	3,450
70	15.0	10,798

The predominant loads are the lateral dead loads, wind drag, and pitching torque. The principal failure modes for analysis are combined flexure and torsion, which result in extreme fiber tensile and shear stresses:

Mode	Stress	Deflection
Flexure	$\theta = \frac{w\ell^2 C_2}{8I}$	$\theta = \frac{w\ell^3}{24\ EI}$
Torsion	$T = \frac{T^1}{2_t A_z}$	$\theta = \frac{T\ell}{KG}$

For the triangular tube:

$$K = \frac{4\,A^2 t}{U}$$

$$U = (b - f_1) + 2\,\frac{(h - f_2 + t)}{\cos\,\alpha}$$

$$A = 1/2\;\;\frac{b\ell}{2} + \frac{b_o \ell_o}{2}$$

Large corner radii are assumed.

Bending shear is also checked for buckling of the flat torque tube sides.

$$\tau_3 = \frac{VAn\bar{y}}{It}$$

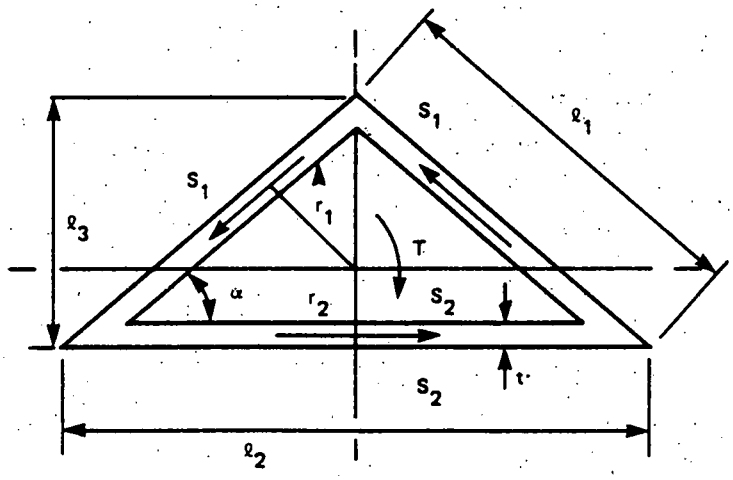

(Dimensions are in inches)

An = area to side of axis

$\bar{y}$ = centroid of area

$= \frac{C1}{2}$ for upper area

$= \frac{C2}{2}$ for lower area

$$A = (69)(0.5) + \left(\frac{2}{3}\right)\left(\frac{69}{0.2}\right)\frac{0.5}{\cos\,\alpha}$$

$$= 34.5 + \frac{11.5}{\cos\,\alpha}$$

By shear flow:

$2S_1 r_1 + r_2 S_2 = T$

$2S_1 \cos \alpha = T - 2S_1 \times (2r_2 \cos \alpha)$

$r_1 = 2r_2 \cos \alpha$

$S_2 = 2S_1 \cos \alpha = T - 2S_1 \times (2r_2 \cos \alpha)$

$$S_1 = \frac{T}{2 \cos \alpha \ (1 + 2 r_2)}$$

$$S_2 = \frac{T}{1 + 2r_2}$$

$$\tau_1 = \frac{S_1}{A_1} = \frac{S_1}{\ell_1 t} \qquad \tau_2 = \frac{S_2}{\ell_2 t}$$

$$C_1 = \frac{h}{3};\ C_2 = h - C_1;\ \alpha = \tan^{-1}\left(\frac{2h}{b}\right);\ \beta = \tan^{-1}\left(\frac{h/3}{b/2}\right)$$

$$f_1 = \frac{t}{\tan \beta};\ f_2 = \frac{t}{\sin \beta};\ I_{xx} = \frac{bh^3}{36} - \frac{b_o h_o^3}{36};\ I_{yy} = \frac{hb^3}{48} - \frac{h_o b_o^3}{48}$$

$$A = \frac{bh}{2} - \frac{h_o h_o}{2};\ J_1 = I_{xx} + I_{yy};\ h_o = h - f_2 - t;\ b_o = b - 2f_1$$

$$A_m = \frac{1}{2}\left(\frac{bh}{2} + \frac{b_o h_o}{2}\right)$$

Table E-7 summarizes the section properties.

Table E-7

SECTION PROPERTIES

ℓ_2 (m)	ℓ_3 (in)	ℓ_0 (in)	C_1 (in)	C_2 (in)	I_{xxx} (in^4)	I_{yy} (in^4)	J (in^4)	Area (in^2)	α (deg)	f_1 (in)	Wt lb/in	A_m (ft^2)
67.26	59.76	58.39	19.92	39.84	37,114	37,114	74,228	102.66	60	0.87	7.78	2,010
65.3	19.92	18.84	6.64	13.28	3,020	27,000	30,100	72.1	30	1.87	5.46	670
66.32	29.88	28.7	9.96	19.92	7,580	30,100	37,700	78.4	40.9	1.34	5.94	991
66.81	39.84	38.58	13.28	26.56	14,600	33,000	47,500	85.72	49.1	1.09	6.50	1,830

Table E-8 summarizes the torque tube torsional shear loads and stresses for various spans, shapes, tube cross sections, and wind conditions.

Table E-8

TRIANGULAR TORQUE TUBE TORSIONAL STRESSES

Span (ft)	Shear Load (lb)			Shear Stress (psi)		
	10 mi/h	39 mi/h	70 mi/h	10 mi/h	39 mi/h	70 mi/h
Case a: $h = 19.92$; $\alpha = 30°$; $\ell_2 = 69$; $r_2 = 6.64$						
20	68.4	1040	3250	1.9	30.1	94
40	136	2080	6510	3.9	60.2	188
80	273	4160	13000	7.9	120	377
Case b: $h = 29.88$; $\alpha = 40.9°$; $\ell_2 = 69$; $r_2 = 9.96$						
20	43.4	659	2060	1.3	19.1	69.8
40	86.7	1318	4130	2.5	38.2	120
80	173	2640	8550	5.0	76.4	239
Case c: $h = 39.84$; $\alpha = 49.1°$; $\ell_2 = 69$; $r_2 = 13.28$						
20	33.0	500	1570	1.9	14.5	45.5
40	65.9	1000	3140	3.8	29.0	91
80	132	2000	6280	7.6	58.1	181
Case d: $h = 59.76$; $\alpha = 60°$; $\ell_2 = 69$; $r_2 = 19.92$						
20	22.2	338	1060	0.6	9.8	30.7
40	44.5	675	2120	1.3	19.6	61.4
80	88.9	1350	4240	2.6	39.2	123

Table E-9 summarizes the torque tube bending stresses and torsional deflections for two cases and wind speeds.

Table E-9

BENDING STRESSES AND DEFLECTIONS

	Length (ft)	Wind (mi/h)	W (lb/in)	T_t (psi)	Θ_t (mr)
Case a:	h = 29.88 in				
	L = (78.4)(0.0785) + 250 + wind = 8.65 + wind				
	$I = 7580\ in^4$				
	$T_t = 18.9\ W$				
	$\Theta_t = 0.175\ W$				
	20	10	8.96	170	0.157
	wt = 1476*	39	13.3	252	0.232
		70	23.67	448	0.413
	40	10	8.96	680	1.256
	wt = 2952*	39	13.3	1208	1.756
		70	23.67	1792	3.304
Case b:	h = 19.92 in, L = (72.1)(0.0785) + 250 + wind = 8.16 + wind				
	$I = 3020\ in^4$				
	$T_t = 31.66\ W$				
	$\Theta_t = 0.0438\ W$				
	20	10	8.47	268	0.371
	wt = 1358*	39	12.8	405	0.561
		70	23.62	733	1.02
	40	10	8.47	1070	2.97
	wt = 2720*	39	12.8	1620	4.49
		70	23.2	2940	8.14

Table E-10 shows the bending shear stresses of the torque tube for various cases.

Table E-10

BENDING SHEAR 70-mi/h WIND

h (in)	A (in^2)	$\bar{y}$ (in)	ℓ (ft)	W (lb/in)	V (lb)	τ (psi)
19.92	47.8	6.64	20	23.2	2780	585
			40		5560	1170
29.88	49.7	9.96	20	23.7	2844	371
			40		5688	742
39.84	52.5	13.3	20	24	2880	275
			40		5760	550
59.76	57.5	19.9	20	25.3	3036	187
			40		6070	374

E.4 Heliostat Steel Spaceframe Sizing

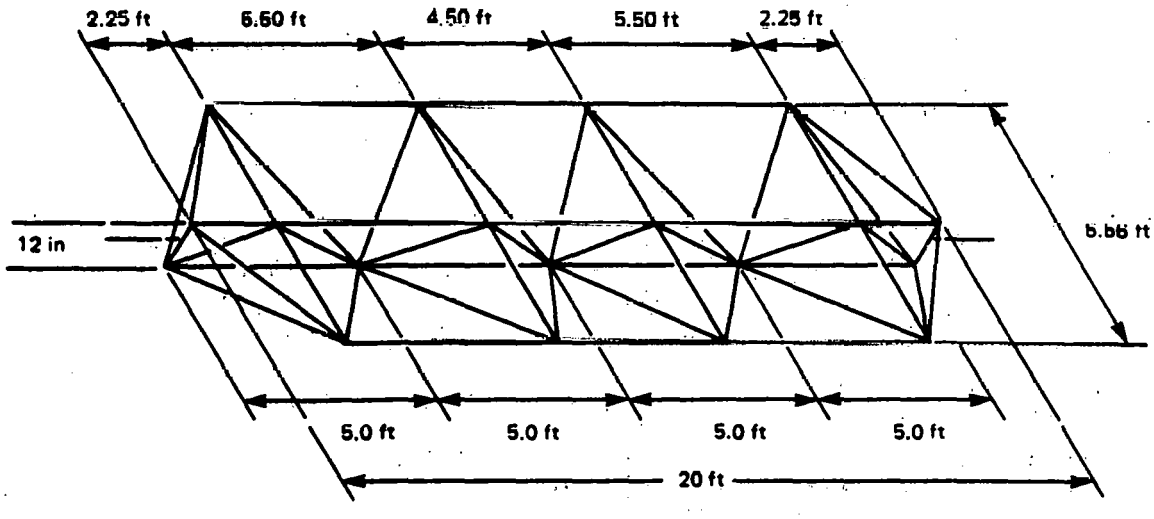

E.4.1 Critical Conditions

The critical conditions for heliostat spaceframe sizing are as follows:

- 50 mi/h wind normal to operation, stress limit
- 13 mi/h wind, deflection limit

E.4.2 Loads

$$w = W_{wind} + W_{structure} + W_{panel}$$

$$= 3.8 \text{ lb/in} + 2.5 \text{ lb/in} + 2.4 \text{ lb/in} = 8.7 \text{ lb/in}$$

For simply supported beam, uniformly loaded

$$M_{max} = \frac{w^2}{8} \quad Z_{required} = \frac{M_{max}}{T_{allow}}$$

Deflection is based on concentrated loads at panel support point:

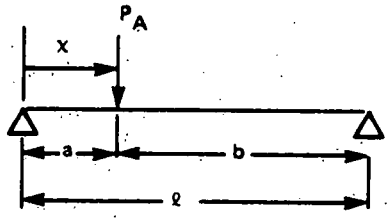

$$y_A = \frac{P_A\, bx}{GEI\ell}\left[2\ell(\ell - x) - b^2 - (\ell - x)^2\right]$$

Maximum slope error due to panel-structure deflection occurs in end panels. In all cases, these deflections resulted in less than 0.1 mr structural deflection (panel-pointing error).

E.4.3 Sizing of Lateral Structural Members

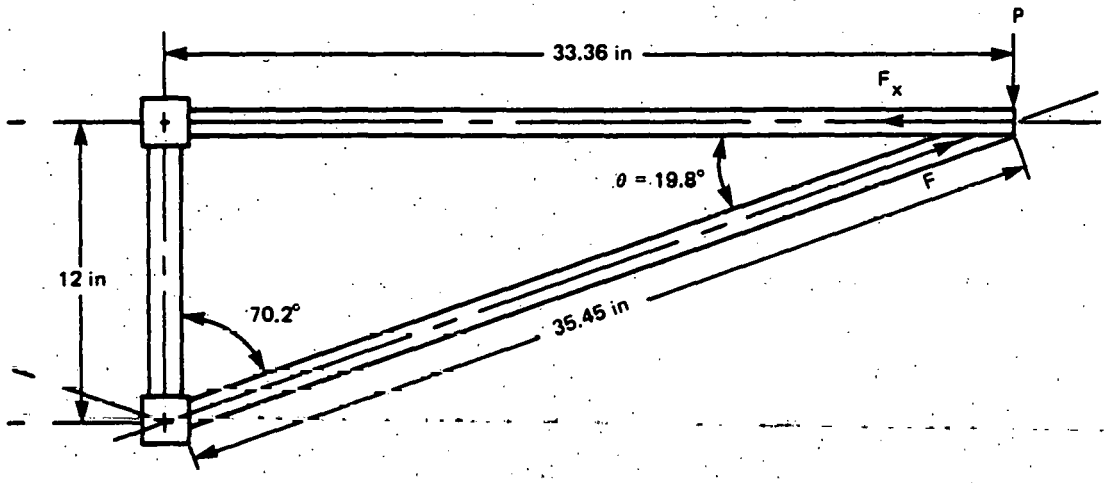

P = panel weight and wind load (for 10-ft panel width)

= (2.88 lb/ft^2) (5 ft x 10 ft) + (3.8 lb/in) (10 ft x 12/2 ft) =

= 372 lb

UTP = 400 lb

$$F = \frac{P}{\sin \theta} = \frac{4 \text{ in}}{\sin 10.8^\circ} = 1180 \text{ lb}$$

For 1 x 1 x 1/16 inch square tubing,

Axial load:

$$\theta = \frac{F}{A} = \frac{1180 \text{ lb}}{1x1 - (0.874)^2} = 9400 \text{ psi}$$

$$P_{CR} = \frac{4\gamma^2 EI}{2} = 32{,}700 \text{ lb (pinned ends)}$$

$$= 8200 \text{ lb (hinged ends)}$$

Panel deflection due to deflection as a result of compression of lower member:

$$\alpha = \frac{P\ell}{EA}\,\frac{\sin 19.8^\circ}{(33.36\text{ in})} = \frac{(1180\text{ lb})\,(35.45)\,(\sin 19.8^\circ)}{(30{\cdot}60^6)\,(0.126\text{ in}^2)\,(33.36)} = 0.1\text{ mr}$$

Table E-11

MINIMUM SECTION MODULUS REQUIRED

Module Length (ft)	M_{max} (in-lb)	Z_{min} @ 15,000 psi (in^3)
20	62,600	4.2
40	250,600	16.8
60	563,400	37.8

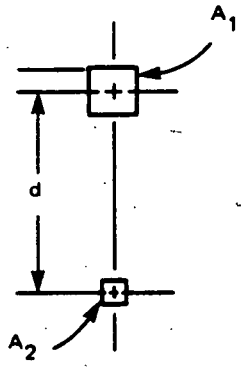

E.4.4 Member Sizing

Assume square tubing for structural members for torsional stiffness required for "thin" overall section of spaceform and ease of fabrication. (Refer to Tables E-12 and E-13.)

Table E-12

SECTION MODULUS REQUIRED

Member Size (in)	Spacing, d (in)	Z (in^3)
2 x 2 x 3/6	12	13.0
3 x 3 x 3/16	12	20
3 x 3 x 1/4	12	25.7
4 x 4 x 1/4	16	46.9

Table E 13

TOTAL FRAME WEIGHT

Item	Description	Size	lb/ft	Length (ft)	lb/unit	Qnty	Total Weight
1	Main member	2x2x3/16	4.31	20	86.2	2	172.4
2	Panel support member	1x1x.063	0.79	5.56	4.39	4	17.57
3	Support diagonals	1x1x.063	0.79	4.04	3.19	12	38.30
4	End brace	1x1x.063	0.79	3.6	2.84	4	11.38
5	End brace diagonal	1x1x.063	0.79	3.71	2.93	4	11.72
6	End main member diagonal	1x1x.063	0.79	2.46	1.94	2	3.88
7	Main member diagonal	1x1x.063	0.79	2.63	2.08	6	12.47
8	Edge member	1x1x.063	0.79	14.5	11.46	2	22.91
9	Bearing post	3x3x1/4	8.80	1	8.80	2	17.6
							308 lb

For 20-tt module: W_T = 308 lb, 15.4 lb/ft or 1.54 lb/ft^2

For 40-ft module: (8.8 lb/ft) (40) (2) = 704 + (135.6) (2)

W_T = 975.2 lb, 24 lb/ft or 2.44 lb/ft^2

For 60-ft module: (12.02 lb/ft) (60) (2) = 1.442.4 + (135.6) (3)

W_T = 1849 lb, 30.8 lb/ft, or 3.08 lb/ft^2

E.5 Heliostat Steel Torque Tube Structure Sizing

Structural sizing for steel torque tubes was based on the following assumptions:

- Minimize weight by designing with nonstandard structural shapes sizes to minimum strength requirements
- Torque tube flexural deflection limited to 5 mr longitudinally and 1 mr laterally, maximum determined at either end
- Rib dimensions based on web buckling

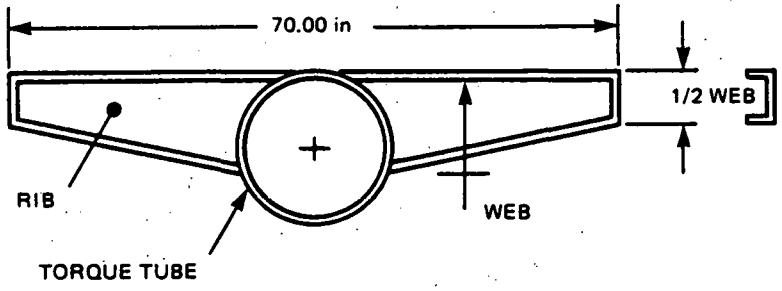

The analysis assumed a simply supported and uniformly loaded beam. Table E-14 shows the steel torque tube deflections for various spans.

E.6 GRC vs Steel Tubular Shape Comparison

The cost of round tubes made of GRC and steel were compared, designed for the same stiffness. The comparison was based on the following assumptions:

- Cost of steel = $0.30/lb
- Cost of GRC = $0.014/lb
- Simply supported beam of 20-, 40- and 60-ft length with concentrated panel loads
- Minimum wall thickness of 0.06-inch steel and 0.5-inch GRC due to manufacturing limitation
- Optimum tube diameter is that for required stiffness at minimum wall thickness

Table E-14

TORQUE TUBE PERFORMANCE

Deflection (mr)	Span Length (ft)	Torque Tube		Rib		Longitudinal Deflection (mr)
		Size (in)	Weight/ft	Web x Thick. (in)	Weight/ft	
0.5	20	8 OD x 0.087	7.4	6 x 0.107	5.23	0.5
0.1	40	15 OD x 0.105	16.8	12 x 0.118	9.77	0.1
0.1	60	22 OD x 0.105	24.6	6 x 0.107	5.23	0.1

Figure E-1 shows the relative cost of the steel and GRC torque tubes as a function of the module size.

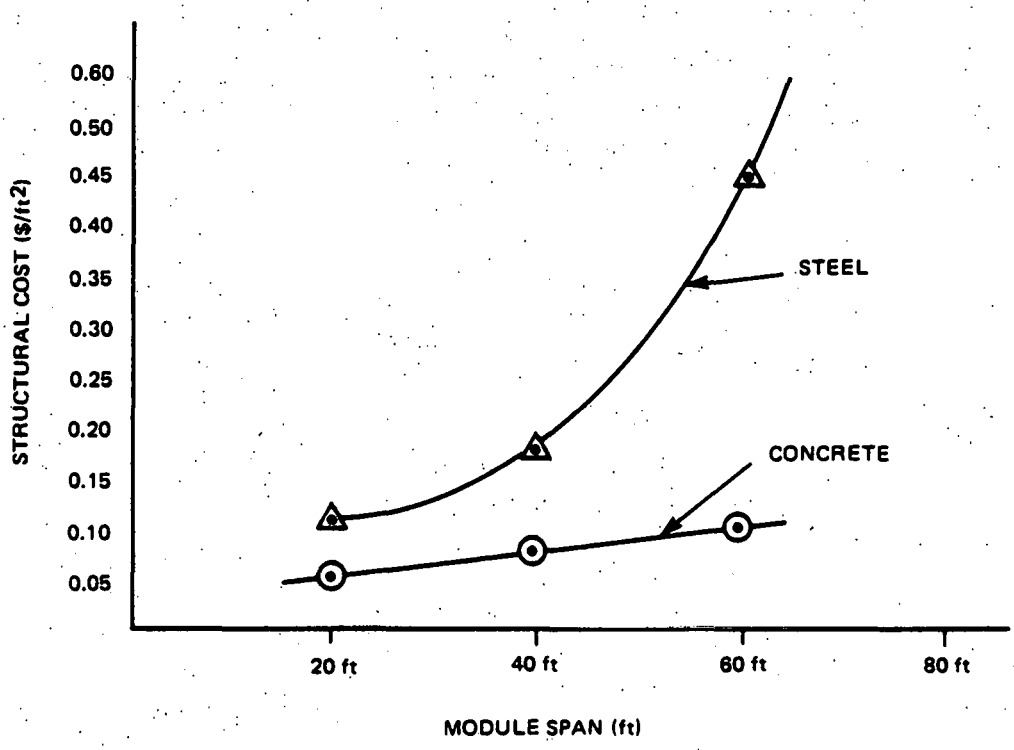

FIGURE E-1 COST COMPARISON CURVE FOR STEEL AND CONCRETE TORQUE TUBES

The concrete cost curve in Figure E-1 does not increase as rapidly as the steel curve because at small sizes the 1/2-inch wall thickness results in an overstiff tube design. Based in part on this comparison, as well as that between the GRC torque tube and steel spaceform, the GRC material was chosen.

E.7 Structure Summary

Table E-15 shows the summary of the cost, weight and longitudinal deflection of the three types of structures considered. Although the weight of the GRC torque tube is greater, its cost and deflection are the least and, therefore, this construction is superior.

Table E-15

OVERALL STRUCTURAL SUMMARY FOR HELIOSTATS

Design	Size (in)	Weight/ft^2	Longitudinal Deflection (mr)	Material Cost ($/ft^2)
Steel torque tube	20 ft length 8 OD x 0.087	1.4	5	0.42
	40 ft length 15 OD x 0.105	2.3	5	0.69
	60 ft length 22 OD x 0.105	3.1	5	0.93
Spaceframe	20 ft length 2 x 2 x 3/16	0.8	1	0.24
	40 ft length 3 x 3 x 1/4	2.4	1	0.72
	60 ft length	3.1	1	0.93
GRC triangular tube	20 ft length	7.5	0.05	0.11
	40 ft length	7.5	0.6	0.11
	60 ft length	7.5	2.2	0.11

★U.S. GOVERNMENT PRINTING OFFICE: 1980-740-145/1054